INTERNATIONAL ATOMIC ENERGY AGENCY
UNITED NATIONS EDUCATIONAL, SCIENTIFIC AND CULTURAL ORGANIZATION
INTERNATIONAL CENTRE FOR THEORETICAL PHYSICS
I.C.T.P, P.O. BOX 586, 34100 TRIESTE, ITALY, CABLE: **CENTRATOM TRIESTE**

H4-SMR 1012 - 10

AUTUMN COLLEGE ON PLASMA PHYSICS

13 October - 7 November 1997

CHAOS IN PLASMAS

ZENSHO YOSHIDA

University of Tokyo, Hongo, Tokyo 113, Japan

These are lecture notes, intended for distribution to participants.

Contents

Chapter 1

Chaotic Motion of Particles

1.1 Chaos in the theory of dynamics

Chaos is a general and abstract notion implying complexity, perplexity, disorder, confusion, etc., and it is difficult to give a clear definition to this subjective idea. In the theory of dynamics, especially in its ideal representation given by Hamilton's canonical form, however, we can characterize "chaos" as the complementary set of ordered motion that is represented by "integrable" equations of motion (Sec. 1.2).

Roughly speaking, an integrable motion can be represented as constant-velocity motion in an appropriate curvilinear coordinates. The simplest example is the motion of a free particle that draws a straight-line orbit in the Cartesian coordinates. Applying appropriate coordinate transformations, we can cast some class of orbits in straight lines in the new coordinates. For example, let us consider a harmonic oscillator, whose Hamiltonian is

$$H = \frac{1}{2}(p^2 + x^2),$$

where p and x are the momentum and position of the oscillator, respectively. The orbit, in the "phase space" p-x, traces out circle given by H = constant. Transforming into polar coordinates

$$P = \left(p^2 + x^2\right)^{1/2}, \quad Q = \tan^{-1}(p/x),$$

the orbit is given by a straight line P = constant ($\sqrt{2H}$), $Q = t$ ($\in \mathbf{R}$) in the phase space of Q-P.

One may consider that all curved orbits can be represented by straight lines by choosing appropriate curvilinear coordinates. If we could find such representation, the equation of motion is really "integrated". Much efforts had been devoted to construct a systematic method of finding such coordinate transformations, before we found fundamental difficulty pointed out by Poincaré. In the next section, we shall give a clear definition of the "integrability", and then discuss non-integrable dynamics, that is the chaos in dynamical systems.

1.2 Integrable system and non-integrable system

Dynamics of a physical system is represented by an orbit (streamline) in the phase space. In this chapter, we consider a dynamical system that has a finite degree of freedom. The phase space is the Euclidean space whose dimension corresponds to the degree of freedom.

Geometrically, a curve in any N dimensional space is defined by the intersection of surfaces. When each of these surfaces moves with a changing parameter(s) (the parameter could be the ordinary time), the curve of intersection will also change as a function of the same parameter(s). The number of these parameters determines the degrees of freedom of the curve. Let us consider a smooth real-number valued function $F(x, y, z)$. For real p, the equation

$$F(x, y, z) = p$$

defines a surface. The set of points (x, y, z) that satisfies the above equation constitutes a *level set* of $F(x, y, z)$ in the x-y-z space. If p is appropriately chosen (i.e. it is in the range of F), and if F is not "degenerate" in the sense that $\partial_x F$, $\partial_y F$ and $\partial_z F$ are non-zero, then we obtain a set of solutions $\{(x, y, z);\ F(x, y, z) = p\}$ with a dimensionality $N - 1 = 2$ for an original $N = 3$. This set, then, defines a two-dimensional surface in the three-dimensional space. The solution of $G(x, y, z) = q$, where $G(x, y, z)$ is another smooth real-valued, and q is a real number, will yield another such two-dimensional set of points (surface). If these two functions are independent in the sense that

$$(\nabla F) \times (\nabla G) \neq 0,$$

then the intersection of the level sets of these (Fig. 1.1), viz., the solution of the set of simultaneous equations

$$F(x, y, z) = p, \quad G(x, y, z) = q$$

will generate a set of $N - 2 = 1$ dimension. This one-dimensional set corresponds to what we commonly understand by a curve.

To determine a curve in an N-dimensional space, we need $N - 1$ independent real-number valued functions $F_j(x_1, \cdots, x_N)$ $(j = 1, \cdots, N)$. The level set of each function defines an $N - 1$ dimensional hyper-surface (manifold).[1] A one-dimensional curve is formed by the intersection of these surfaces, and is obtained by solving $F_j(x_1, \cdots, x_N) = p_j$ $(j = 1, \cdots, N)$ simultaneously. We are thus able to demonstrate that given an appropriate set of functions $F_j(x_1, \cdots, x_N)$ $(j = 1, \cdots, N)$, we can always find a one-dimensional set of points (a curve) common to them all.

Let us now consider the inverse problem. For a given smooth curve in an N-dimensional space, can we find an appropriate set of functions $F_j(x_1, \cdots, x_N)$ $(j = 1, \cdots, N)$ such that the intersection of their level sets coincides with the given curve? As far as we consider this problem "locally", the answer is yes. Let P be a point on the curve. We consider a neighborhood V of P where the curve looks like a straight line. Changing the coordinates to align the x_N

[1] For example, we can solve $F_1(x_1, \cdots, x_N) = p_1$ for x_1, in a neighborhood of a regular point $(\partial F(x_1, \cdots, x_n)/\partial x_1 \neq 0)$, we obtain the implicit function $x_1 = f_1(x_2, \cdots, x_n)$. This one-dimensional relation among the variables defines a hyper-surface.

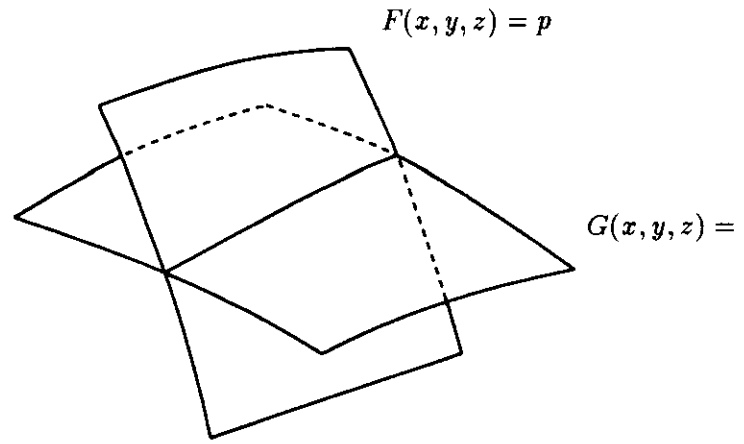

Figure 1.1: Intersection of two surfaces defines a curve in three-dimensional space.

axis to be parallel to the line, we obtain the equations $x_j = p_j$ (constant) $(j = 1, \cdots, N-1)$ whose simultaneous solution represents the curve locally in V. In trying to solve the "global" problem, however, we meet the following difficulty. The global problem consists in finding the hyper-surfaces that include the curve throughout their trajectory. For a curve that moves about in a certain domain of space, such hyper-surfaces must have a highly complicated structure. In fact, for a sufficiently complex dynamics, well-defined smooth hyper-surfaces that contain the complicated streamlines may not actually exist. This thought experiment gives us a glimpse of the pathway leading to the concept of "chaos" in dynamical systems.

For a dynamical system, the existing of functions defining hyper-surfaces implies existence of the constants of motion, because the fact that the orbit stays on a hyper-surfaces $F_j(x_1, \cdots, x_N) = p_j$ implies that this p_j is a constant of motion. A search for such functions is an essential part of the theory of dynamical systems. We revisit this problem from the view point of Hamiltonian dynamics.

Note 1 (Hamiltonian system) *Because of its special form, the Hamiltonian flow has less degrees of freedom than a general incompressible flow. Let us see how? To determine a curve in an N-dimensional phase space, we need a total of $N-1$ conservation laws (hyper-surfaces). For a stationary Hamiltonian flow in a $N = 2\nu$ (ν is the number of space dimensions) phase space, on the other hand, we need only ν independent conservation laws. The universal validity of this assertion can be seen as follows: Let us assume that all momenta $p_1, \cdots, p_\nu$ are constants of motion. We can transform the coordinates so that only p_ν remains non-zero. Then Hamilton's equations*

$$\frac{d}{dt}x_j = \frac{p_j}{m} = 0 \quad (j = 1, 2, \cdots, \nu - 1),$$

generate a new set of constants x_j = constant $(j = 1, 2, \cdots, \nu - 1)$, which, when added to the original ones, make a total of $2\nu - 1 = N - 1$ conservations laws. The argument can be

generalized to the case when the ν independent conserved quantities F_j are combinations of the momenta and the coordinates, such that their Poisson bracket vanishes,

$$\{F_k, F_\ell\} = 0 \quad (\forall k, \ell). \tag{1.1}$$

This result is known as "Liouville's theorem".

When we have a sufficient number of conservation laws, the particle orbits or the streamlines of the flow can be readily and uniquely (for given initial conditions) computed. A dynamics of this variety is called *integrable*. Note that the present concept of the integrability is different from the conventional notion of the solvability of ODE's. It means that we can solve the problem using conservation laws.

Looking for conservation laws is the first and foremost duty of every physicist. The basic idea behind finding conservation laws for a given system is to find appropriate curvilinear coordinates on which the curved orbits become straight lines (the standard action-angle approach). If this effort were to be successful, the constancy of all "momenta" in the new coordinate system would provide all the conservation laws needed to specify the streamlines.

The study of the three-body problem led us to notice that some complicated dynamics, that are close to a periodic motion, do not allow us to find such transformations and hence the desired conservation laws. We had shown in the preceding section, that it was always possible (in an abstract geometrical sense) to find the required transformations "locally". What has changed is that we now seek a global expression of the conservation laws. And it is precisely for the global description of the near-periodic but complex behavior, that the relevant conservation laws defy discovery. This class of complex dynamics, which is inherently "non-integrable", goes under the popular name *chaos*.

In the following sections, we will discuss explicit examples of chaos in plasma systems.

1.3 Example I (magnetic field-line chaos)

1.3.1 Canonical form of magnetic field-line equations

In three-dimensional space ($\mathbf{R}^3$), by a skillful representation of the magnetic field (or any general divergence-free vector field), we can cast the field line equations into a canonical (Hamiltonian) form. For a given magnetic field $\boldsymbol{B}(\boldsymbol{x}, t)$, the field line equation is

$$\frac{d}{d\tau}\boldsymbol{x} = \boldsymbol{B}(\boldsymbol{x}, t), \tag{1.2}$$

where τ is an abstract variable that indicates the position on the streamline. This τ and the time t are totally different; the magnetic field line is determined for each individual time. Hence, in (1.2), t is regarded just as an independent parameter, just a label. In this section, we omit t to simplify notation. Considering τ as an "artificial time", the field line equation (1.2) can be regarded as a streamline equation for a steady (τ-independent) flow $\boldsymbol{B}$.

We begin with the simpler case, in which $\boldsymbol{B}(\boldsymbol{x})$ is homogeneous with respect to z, one of the trio forming the Cartesian coordinates x-y-z. Because of this symmetry, and of the divergence-free property of $\boldsymbol{B}(\boldsymbol{x})$, we can write $\boldsymbol{B}(\boldsymbol{x})$ in the form

$$\boldsymbol{B}(x,y) = \nabla\psi \times \nabla z + B_z \nabla z \tag{1.3}$$

where $\psi(x,y)$ and $B_z(x,y)$ are two scalar functions. From (1.3), we deduce

$$\boldsymbol{B} \cdot \nabla\psi = (\nabla\psi \times \nabla z) \cdot (\nabla\psi) + B_z(\nabla z) \cdot (\nabla\psi) \equiv 0, \tag{1.4}$$

implying that the vector field $\boldsymbol{B}(\boldsymbol{x})$ is tangential to a level set of the function $\psi(x,y)$.[2] Hence, ψ is constant along the streamline of the flow (magnetic filed) $\boldsymbol{B}(\boldsymbol{x})$, viz., ψ is a constant of motion of the dynamics defined by $\boldsymbol{B}(\boldsymbol{x})$.[3]

We have, thus, shown that every streamline of an incompressible stationary flow (such as a magnetic field) with an "ignorable coordinate" must be integrable, and its trajectory must degenerate on a smooth curve in $\mathbf{R}^3$. This important result can also be derived as a straight forward implication of Hamiltonian dynamics. For $\boldsymbol{B}(\boldsymbol{x})$ of (1.3), the x and y components of the streamline equation become

$$\begin{cases} \dfrac{dx}{d\tau} = \partial_y \psi, \\ \dfrac{dy}{d\tau} = -\partial_x \psi, \end{cases}$$

which read as Hamilton's equations of motion with the coordinate x, the momentum y, and the Hamiltonian $\psi(x,y)$. In this two dimensional phase space, one integral of motion suffices for integrability, and we have already shown that the Hamiltonian ψ is a constant of motion. The integral surfaces (curve) of this system are the level sets of ψ.

Note 2 (canonical form of 3D field-line equations) *Consider a three-dimensional incompressible field $\boldsymbol{B}(\boldsymbol{x})$ in a toroidal domain Ω ($\subset \mathbf{R}^3$) (see Fig. 1.2).*

Such a vector field can be represented in the form[23]

$$\boldsymbol{B} = \nabla\Psi \times \nabla\zeta - \nabla\chi \times \nabla\vartheta, \tag{1.5}$$

where ζ and ϑ are, respectively, the appropriate toroidal and poloidal angles (1.2), and Ψ and χ are scalar functions of ζ, ϑ and ξ (a radial coordinate). Since

$$\nabla\Psi \times \nabla\zeta - \nabla\chi \times \nabla\vartheta = \nabla \times (\Psi\nabla\zeta - \chi\nabla\vartheta),$$

[2]The level set in the x-y-z space of $\psi(x,y)$ is a column whose section by an x-y plane is the contour curve of $\psi(x,y)$ in the plane.

[3]In the magnetic fusion parlance , (1.4) is called the magnetic differential equation, and the function ψ is called a surface quantity. The field-line traces a surface in three space, and ψ, by virtue of its constancy, can serve as a label for the surface. For a geometry of such nested surfaces, ψ becomes a convenient "radial" (orthogonal to the surface) coordinate.

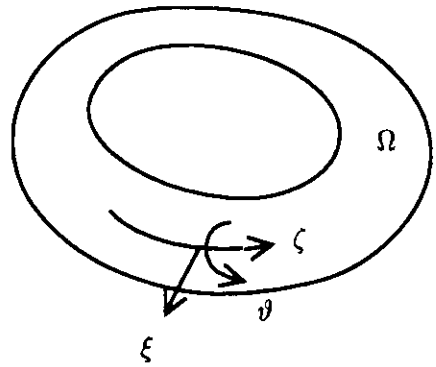

Figure 1.2: Toroidal curvilinear coordinate (ξ, ϑ, ζ).

Ψ and χ are really nothing but the toroidal and poloidal components of the vector potential. Due to the gauge freedom, we need only two independent components of the vector potential to uniquely determine the electromagnetic fields.

If we replace the radial coordinate ξ by the function χ, and assume that the Jacobian

$$\frac{D(\chi, \vartheta, \zeta)}{D(x, y, z)} = \nabla\chi \cdot (\nabla\vartheta \times \nabla\zeta) \neq 0$$

(with the implication that the streamline does not turn back in circulating the toroidal domain), the streamline equations read

$$\begin{cases} \dfrac{d\vartheta}{d\zeta} = \dfrac{\nabla\vartheta \cdot \boldsymbol{B}}{\nabla\zeta \cdot \boldsymbol{B}}, \\ \dfrac{d\chi}{d\zeta} = \dfrac{\nabla\chi \cdot \boldsymbol{B}}{\nabla\zeta \cdot \boldsymbol{B}}. \end{cases} \tag{1.6}$$

After using (1.5) to evaluate the right-hand side of (1.6), we obtain the set of canonical equations

$$\begin{cases} \dfrac{d\vartheta}{d\zeta} = \partial_\chi \Psi, \\ \dfrac{d\chi}{d\zeta} = -\partial_\vartheta \Psi, \end{cases} \tag{1.7}$$

for which the toroidal angle ζ parallels time, the poloidal angle ϑ, is the angle coordinate, χ, mimics the canonical momentum (action variable), and $\Psi = \Psi(\chi, \vartheta, \zeta)$ plays the role of the Hamiltonian.

For a general flow (magnetic field), the Hamiltonian $\Psi(\vartheta, \chi, \zeta)$ depends on all three of its arguments, i.e, there is no ignorable coordinate and hence no constant of motion. The Hamiltonian system (1.7), then, is not integrable. If Ψ were independent, say, of the toroidal angle ζ, a constant of motion will emerge, and the system (1.7) becomes integrable.

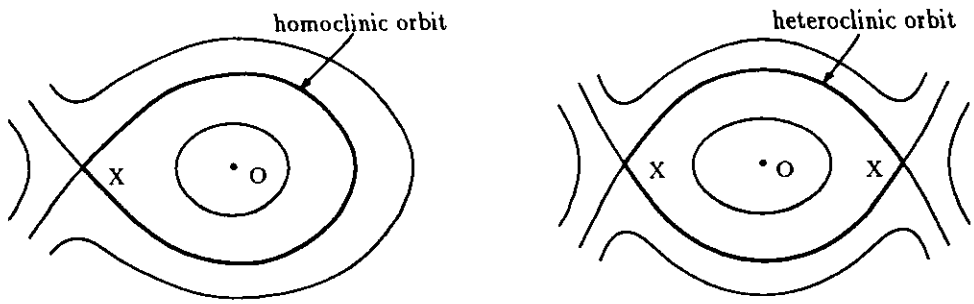

Figure 1.3: Homoclinic orbits and heteroclinic orbits.

1.3.2 Poincaré map and perturbation

If we assume $B_z \equiv 0$, then the critical points of $\psi(x, y)$ gives the null points. Since $\boldsymbol{B}$ is homogeneous in the direction of z, the null points generates a straight line in the direction of z. Critical points of $\psi(x, y)$ are classified into "O points", that are the maximum or minimum points of $\psi(x, y)$, and "X points" that are saddle points. The O points are isolated from field lines (contours of $\psi(x, y)$), while there are normally four field lines that are connected to each X point. For a given sense of τ, two of the curves converge to the X point, while the other two curves diverge. We call the former, the stable orbits, and the latter, the unstable orbits.

If an unstable orbit does not escape from a certain bounded region in the phase space x-y, this curve must be connected with a stable orbit (Fig. 1.3), as far as the representation (1.3) holds. There are two possibilities; One is the case when the unstable orbit starting from an X point comes back to the same X point. Such a closed orbit is called a homoclinic orbit. The other is the case when the unstable orbit is connected to another X point. This curve is called a heteroclinic orbit. When we break the symmetry (homogeneity) with respect to z, these homoclinic and heteroclinic orbits are strongly deformed, resulting in "Chaos". Field-line chaos stems in the neighborhood of X points. To see this, we first consider an abstract model of perturbed Hamiltonian system.

Let us consider a Hamiltonian system which is perturbed by a periodic potential of period T;

$$\frac{d}{d\tau}\begin{pmatrix} x \\ y \end{pmatrix} = \begin{pmatrix} \partial_y \tilde{\psi} \\ -\partial_x \tilde{\psi} \end{pmatrix} \quad (\tilde{\psi}(x, y, \tau) = \psi(x, y) + \epsilon f(x, y, \tau)). \tag{1.8}$$

The perturbation is assumed to be of the order of ϵ (≥ 0). When $\epsilon = 0$, (1.8) becomes autonomous.

We consider a streamline (orbit) starting from an initial point $\boldsymbol{x}_0$, and take a series of periodic points $\{\boldsymbol{x}_0, \boldsymbol{x}(T), \boldsymbol{x}(2T), \cdots\}$. Denoting

$$\boldsymbol{x}((n+1)T) = P\boldsymbol{x}(nT),$$

we define a mapping P. Since the system (1.8) is periodic in t of period T, this P does not

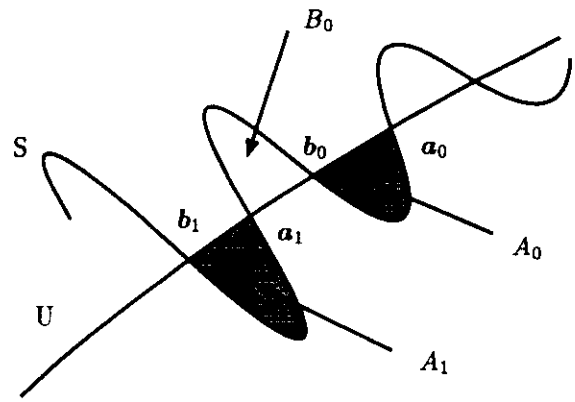

Figure 1.4: Intersection of stable curve (S) and unstable curve (U).

depend on t explicitly, i.e., P determines a temporally discrete autonomous system. We call P the *Poincaré map.*

The discrete mapping P produces series of points on the surface of the two-dimensional phase space. Obviously, when $\epsilon = 0$, the series of points are included in the level set (contour curve) of the unperturbed Hamiltonian $\psi(x, y)$. Choosing different initial values, we can construct the total structure of the contours of $\psi(x, y)$. In a perturbed system ($\epsilon > 0$), the total Hamiltonian $\tilde{\psi}(x, y, t)$ is no longer a constant of motion, and hence the behavior of streamlines can become very complex. Let us investigate the complex structure by using the discrete mapping P.

If there exists a periodic streamline of period T, a point on this curve is a fixed point of P. This fixed point is classified into O and X points by studying the eigenvalues of the linearized mapping L of P. When L (2×2 matrix) has two real eigenvalues, the fixed point is an X point. The two lines that parallel the two real eigenvectors are invariant under the operation of L, and hence, points move on these lines in the neighborhood of the X point. The X point is the accumulation point of these series of points. The converging curve, with respect to the X point, is called a stable curve (denoted by S), and the diverging curve is called an unstable curve (U). These curves contain many different series of points that have different origins. Therefore, S and U do not necessarily connect smoothly. They may intersect each other.

When S and U intersects at one place, say $\boldsymbol{a}_0$, then infinite number of intersections occur. Indeed, the mapped point $P\boldsymbol{a}_0 = \boldsymbol{a}_1$ must be on S as well as on U. Therefore, S and U intersects at $\boldsymbol{a}_1$ (Fig. 1.4). Repeating the mapping, we obtain infinite set of intersections at points $P^n\boldsymbol{a} = \boldsymbol{a}_n$ ($\forall n \in \boldsymbol{Z}$).

The intersections of S and U yields a series of closed domains as shown in Fig. 1.4. All points included in the area A_0 are mapped into A_1 by applying P. By the incompressibility of the canonical transform P, the area of A_1 is equal to that of A_0. We can define the sense of the

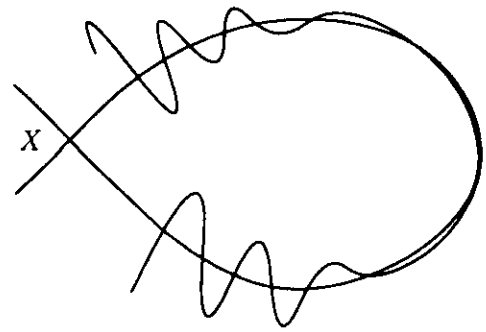

Figure 1.5: Area conservation of intersecting curves.

domain by the orientation of the order of points on the boundary. The P conserves this sense of the domain, as well as the area (Liouville's Theorem). If A_0 were mapped to B_0, this sense flips, and hence, we see that A_0 must be mapped to A_1. Therefore, between $\boldsymbol{a}_0$ and $P\boldsymbol{a}_0 = \boldsymbol{a}_1$, there exists another intersection $\boldsymbol{b}_0$.

If the series of intersection points $P^n\boldsymbol{a}$ and $P^n\boldsymbol{b}$ converges to the X point as $n \to \infty$, the intervals between adjacent points diminished to zero. To keep the area of each domain bounded by S and U, the amplitude of deviation between S and U increases (Fig. 1.5). Therefore, the behavior of points near the X point becomes "chaotic".

1.3.3 Symmetry breaking

Now, we consider the symmetry breaking of magnetic field, and observe the onset of magnetic field-line chaos in the X point.

We consider a magnetic field given by the ABC flow;

$$\boldsymbol{B} = \begin{pmatrix} A\sin\lambda z + C\cos\lambda y \\ B\sin\lambda x + A\cos\lambda z \\ C\sin\lambda y + B\cos\lambda x \end{pmatrix}. \tag{1.9}$$

where A, B, C and λ are real constants. Since this $\boldsymbol{B}$ is periodic in x, y and z of period $2\pi/\lambda$, we consider that a cubic domain of side length $2\pi/\lambda$ be a periodic domain (we can identify every $x + 2n\pi$, $y + 2n'\pi$ and $z + 2n''\pi$ $(n, n', n'' \in \boldsymbol{Z})$ with the fundamental domain $0 \le x, y, z < 2\pi$).

First we assume that $A = 0$. Then, $\boldsymbol{B}(x, y)$ is two dimensional. By defining

$$\psi(x, y) = \lambda^{-1}(B\cos\lambda x + C\sin\lambda y),$$

we can write (1.9) in the form of

$$\boldsymbol{B} = \nabla\psi \times \nabla z + \lambda\psi\nabla z, \tag{1.10}$$

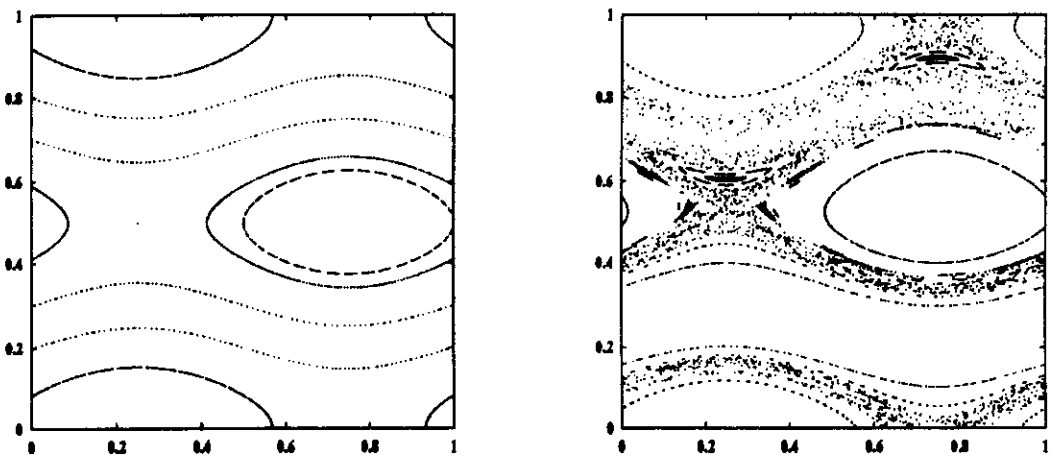

Figure 1.6: Poincaré plot for the ABC flow; (a) $B = 1, C = 0.3, A = 0$, (b) $B = 1, C = 0.3, A = 0.2$ (after Y. Yamakoshi).

(see (1.3)). Therefore, this $\psi(x,y)$ is the Hamiltonian of the corresponding field-line equation.

If none of A, B and C are zero, $\boldsymbol{B}(x,y,z)$ is three dimensional. The z-dependent term introduces a periodic perturbation of period $2\pi/\lambda$. Plotting the cross point of each field line at the surface $z = 0$, we obtain the Poincaré mapping (see Fig. 1.6). In Fig. (a) the parameter A is zero. We observe that points move on the contours of the unperturbed Hamiltonian $\psi(x,y)$. We observe X points between ellipses of circulating points. In Fig. (b), we plot the perturbed (three-dimensional) Poincaré maps. In the neighborhood of the original (unperturbed) X point, chaotic plots are obtained.

1.4 Example II (particle motion chaos)

1.4.1 Motion of charged particles

Nonlinearity stems in the equation of motion of a charged particle from the spatial inhomogeneity of electromagnetic fields. The "magnetic null point" yields a strong enough nonlinearity to generate "chaos" of the particle motion. The chaotic motion of electrons brings about rapid production of entropy, resulting in efficient heating of electrons at a low-collisionality regime. This nonlinear process can be applied to plasma production that meets the increasing demand for low-gas pressure plasma source suitable for the use in ultra-fine etching of semiconductors. Moreover, this effect may play an important role in high-temperature plasmas such as solar corona, geo-tail and fusion plasmas. The magnetic null point is the place where the magnetic field lines can reconnect if there is a finite resistivity (equivalent to the magnetic diffusivity). In many different examples, the conventional "collisional resistivity", that is deduced by evaluating the scattering of current-carrying electrons by field particles, is very small and it cannot account for the actual reconnection rates. Some mechanisms have been studied to obtain an "anomalous resistivity", including the possibility of the effect of the chaos.

We will start with a pure collision-less model, and show that the mixing effect of chaos yields a rapid production of (kinetic) entropy. This process, however, in transient, and the heating saturates after a short time. As the second step, we will study the effect of collisions with neutral particles. By inelastic collisions of excitation and ionization, that have threshold energies, the electrons lose the energy. This process opens a "sink" for the energy at a high-energy region of the velocity space. A steady state is achieved when the same amount of electrons are provided at a low energy region, and they "cascade" towards the sink. [4] The intermediate energy range can be approximated by the collision-less model. The chaos accelerates the cascade, and hence the energy dissipation is enhanced. In that the nonlinearity enhances the dissipation, the role of chaos represents a generic characteristics of nonlinear dynamics common to the turbulence and self-organization phenomena. The following analysis gives a proof for the above-mentioned scenario, and derives a quantitative estimate of the enhanced resistivity. We will see that the chaos effect can yield a sufficiently large resistivity.

[4] In a real system, the ionization produces low-energy electrons. They are lost by recombination and spatial diffusion. In the present work, we simplify the production and loss of electrons by a probabilistic process under the constraint on the total number of electrons.

We consider the motion of an electron that obeys Newton's equation of motion;

$$m\frac{d^2}{dt^2}\boldsymbol{x} = -e\left[\boldsymbol{E} + \left(\frac{d}{dt}\boldsymbol{x}\right) \times \boldsymbol{B}\right], \tag{1.11}$$

where m is the electron mass, e is the elementary charge, $\boldsymbol{E}$ and $\boldsymbol{B}$ are the electric field and magnetic field, respectively. If $\boldsymbol{E}$ and $\boldsymbol{B}$ are spatially homogeneous, (1.11) is linear with respect to $\boldsymbol{x}$. For example, let us assume that $\boldsymbol{B}$ = constant and $\boldsymbol{E} = \boldsymbol{E}_0 \sin(\omega t)$ ($\boldsymbol{E}_0$ = constant). If the frequency ω is not resonant with the cyclotron frequency $\omega_c = eB/m$, the particle motion is periodic, and hence "heating" cannot occur. We may appeal to some mechanism, besides the resonance, to "disorder" the periodic motion and heat electrons. Collisions are the most simple process to randomize the phase of oscillation of the particle, resulting in non-zero average of energy transfer from the electric field into the particle motion. The other possible process is the chaos, that is a deterministic dynamical process producing complex orbits of particles. Here, we consider a strongly inhomogeneous magnetic field that makes (1.11) nonlinear with respect to $\boldsymbol{x}$. Once the adiabatic invariance of the magnetic moment is destroyed in such an inhomogeneous field, the degree of freedom increases enough to obtain chaotic motion of electrons.

We formulate a slab plasma model assuming, in Cartesian coordinates,

$$\boldsymbol{B} = Jx\begin{pmatrix}0\\1\\0\end{pmatrix}, \quad \boldsymbol{E} = E_0 \sin(\omega t)\begin{pmatrix}0\\0\\1\end{pmatrix}, \tag{1.12}$$

where J is a constant number (J/μ_0 has the dimension of current density; μ_0 is the vacuum permeability). This J and the frequency ω characterize the spatial and temporal scales, respectively. The length scale is defined as follows. For the given ω, the cyclotron-resonant magnetic field B is given by solving $\omega = eB/m$ for B. This resonant magnetic field occurs at $x = L \equiv m\omega/(eJ)$. We define normalized time and coordinates as

$$\hat{t} \equiv \omega t, \quad \hat{\boldsymbol{x}} \equiv \frac{\boldsymbol{x}}{L}.$$

The equation of motion (1.11) now reduces into

$$\hat{x}'' = -\frac{\hat{x}^3}{2} + [F(\hat{t}) + C]\hat{x}. \tag{1.13}$$

Here $'$ denotes the normalized temporal derivative ($d/d\hat{t}$),

$$F' = \hat{E} = \frac{Je^2E}{m^2\omega^3} = \frac{eE}{mL\omega^2},$$

and C is a constant determined by the initial velocity $\hat{z}'$; To derive (1.13), we have used the z-component of (1.11) that reads, after integrating with respect to $\hat{t}$,

$$\hat{z}' = -\frac{\hat{x}^2}{2} + F + C.$$

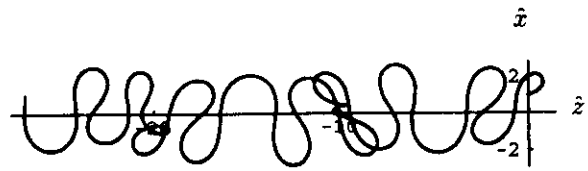

Figure 1.7: The disordered meandering motion of an electron in the neighborhood of the magnetic null point ($\hat{x} = 0$).

In the y-coordinate, the particle moves with a constant velocity.

The nonlinear equation (1.13) becomes "most nonlinear" when all terms have the same order of magnitudes. [5] As a numerical example, let us assume a radio-frequency (RF) electric field with $\omega = 2\pi \times (13.56 \times 10^6)$ sec^{-1} and $E_0 = 10^3$ V/m. When the length scale of $\boldsymbol{B}$ is $L = 2.4 \times 10^{-2}$ m, then we obtain the normalized electric field $\hat{E} = a \sin \hat{t}$ with an amplitude $a = 1$.

When $a = 0$, the energy (Hamiltonian) of the particle conserves, and hence, the nonlinear equation (1.13), whose degree of freedom is one, is integrable. The particle describes a "meandering" orbit in the neighborhood of the magnetic null point ($\hat{x} = 0$). A finite electric field ($a \neq 0$) changes the energy, resulting in non-integrable (chaotic) motion. Figure 1.7 shows a typical orbit of an electron put in an electric field with $a = 1$. The initial energy of this particle is zero. We observe that the typical length scale of the "disordered meandering" is of order unity ($O(L)$ in the physical unit).

1.4.2 Entropy production by chaos

Let us describe some numerical diagnostics of the chaos. The Lyapunov exponent is about 0.2 for $a = O(1)$, which implies that neighboring particles decorrelate after about five periods of oscillations of the RF electric field. In Fig. 1.8, we show the Poincaré plot on the phase space $\hat{x}$-$\hat{x}'$. The orbit covers almost densely over a region in the phase space. The kinetic entropy can be defined by $S = -\sum_\ell p_\ell \log p_\ell$, where p_ℓ is the probability of making a visit at a cell, labeled by ℓ, in the phase space. In Fig. 1.9, we compare the increase of S for the chaotic motion and periodic motion ($\boldsymbol{B} = 0$). While S for the periodic motion achieves a small constant value after a short time, [6] that for the chaotic motion continues to increase. The rapid increase in S is due to the "mixing effect" of the chaos (Fig. 1.8). The rate of the mixing is of the order of the Lyapunov exponent. After the first rapid increase, S goes up slowly. In this slow phase, the

[5] When $|\hat{x}| \gg 1$, we may write $\hat{x} = \hat{x}_0(1 + \tilde{x})$ with a constant $\hat{x}_0$ and $|\tilde{x}| \ll \mathcal{O}(1)$, and the nonlinear term of (1.13) is linearized as $-\hat{x}^3/2 \approx -\hat{x}_0^3(1 + 3\tilde{x})/2$. Then, the drift motion of magnetized particle occurs. Similarly, when $|F| \gg 1$, the linear term $F\hat{x}$ dominates the dynamics, and hence the particle motion recovers the regularity.

[6] The absolute value of S depends on the division of the phase space into cells. Since the periodic orbit is measure zero, the corresponding S converges to zero in the limit of zero cell scale.

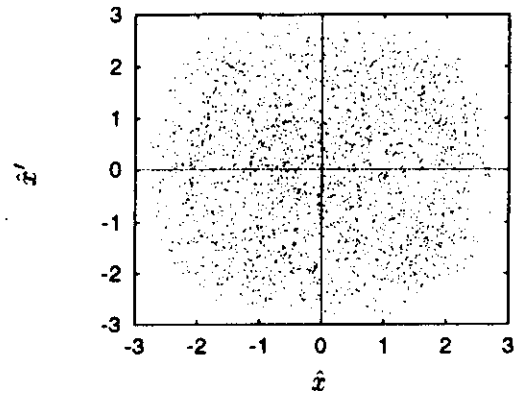

Figure 1.8: The Poincaré plot in the case of $a = 1$.

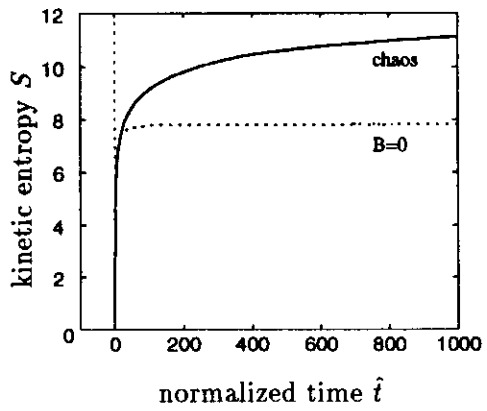

Figure 1.9: Increase of the kinetic entropy S. Here, $a = 1$.

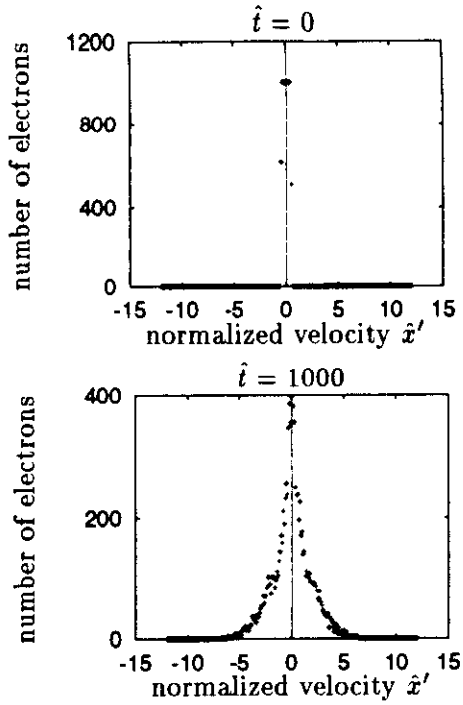

Figure 1.10: Heating of electrons by the chaos.

domain, over which the orbit moves, does not expand appreciably, so that the average energy of the particle is almost saturated.

1.4.3 Collision-less heating by chaos

Figure 1.10 shows the velocity distribution of 10^4 particles. Each particle has different initial condition, but obeys the same equation of motion (1.13), viz., there is no mutual interactions such as collisions or collective motions. However, we observe that a small variation in the initial state expands to create almost Gaussian distribution. While the oscillating electric field is constantly applied, we find that the total energy of many particles approaches to a constant vale. The statistical equilibrium may be regarded as a canonical ensemble. As we have seen in Fig. fig:Poincare, the motion of a particle is approximately ergodic, and hence, the Gibbs distribution can be deduced from the equal probability in the phase space.

In the above calculations, we have seen an essential difference between the collision and the chaos. In the above model, we assumed no process of energy loss, while we applied the RF electric field constantly. If collisions are the mechanism of entropy production, unceasing heating of electrons must occur.

We estimate the effective resistivity by the total change of the energy. In Fig. 1.11, we show that the effective resistivity is enhanced by the mixing effect of chaos by factor 10^2 in comparison

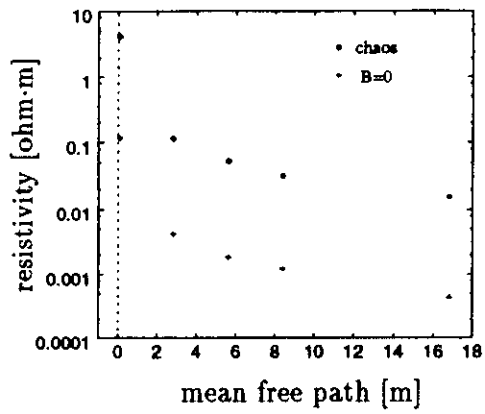

Figure 1.11: Effective resistivities ($n_e = 10^{16}$ m^{-3}).

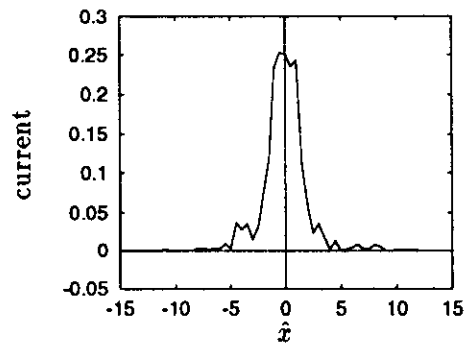

Figure 1.12: Spatial distribution of the current density (the resistive component).

with the case of $\boldsymbol{B} = 0$.

Figure 1.12 shows the spatial distribution of the dissipative current density (the current density that has the same phase of the RF electric field).

Chapter 2

Chaotic Oscillations in Plasmas

2.1 Chaotic time-series produced by a simple dynamical law

Some toy models of mathematical science demonstrated that some simple low-dimensional (i.e., low degree of freedom) dynamical system can produce chaotic solutions. These findings give us motivation of searching a simple dynamical law to account for observed complex data.

Roughly speaking, we mean by "chaotic behavior" the difficulty of predictions. Even if model equations provide deterministic description of temporal evolution, the prediction is difficult when the solution has a high sensitivity to small variation in initial conditions. However, this is not a complete definition of chaos. Consider a linear model

$$\frac{d}{dt}x = \alpha x, \quad x(0) = x_0 \tag{2.1}$$

with $\alpha > 0$. The solution $x(t) = e^{t\alpha}x_0$ is unstable and a small variation in the initial value x_0 expands exponentially, while this system does not have any complexity. Chaos develops in a bounded domain of the phase space; the state variable does not escape from an certain domain. In this sense, chaos has two different aspects, instability and stability. Co-existence of these two characters is possible in nonlinear systems. Let us revisit some well-known examples.

If we modify the growth rate α of (2.1) to a function of x, we obtain a nonlinear model. For example, let us assume a saturation effect and put $\alpha = a(1 - bx)$. Then, we obtain the so-called logistic model

$$\frac{d}{dt}x = a(1 - bx)x, \quad x(0) = x_0. \tag{2.2}$$

Although (2.2) is non-linear, we can "linearize" it by transforming x to $y = b - x^{-1}$;[1] we obtain

$$\frac{d}{dt}y = -ay, \quad y(0) = b - x_0^{-1}. \tag{2.3}$$

We can solve (2.3) as $y(t) = e^{-at}y_0$, and hence, we obtain $x(t) = (b - e^{-at}y_0)^{-1}$. Since (2.3) has a negative time-constant $-a$, the solution of the nonlinear model (2.2) is basically stable.

[1] This is not a "linear approximation", but is a rigorous transformation.

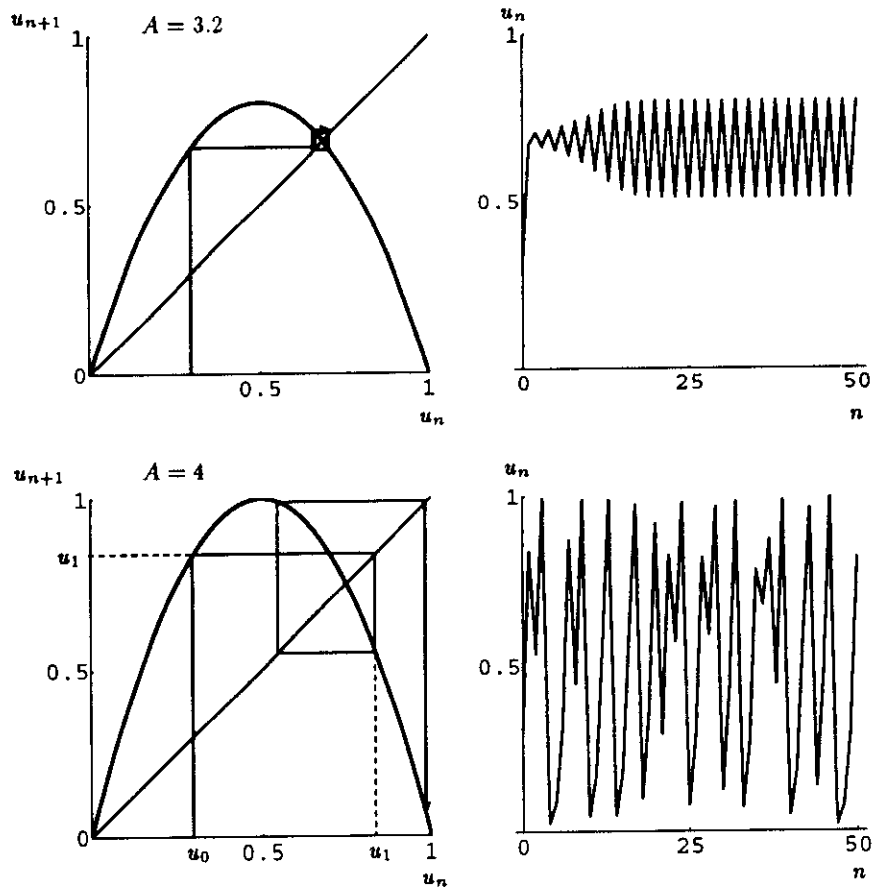

Figure 2.1: Logistic map for $A = 3.2$ and $A = 4$.

Chaos occurs when we discretize time in (2.2). Let us consider a finite difference equation

$$x_{n+1} - x_n = a(1 - bx_n)x_n, \tag{2.4}$$

which defines the famous "logistic map"

$$u_{n+1} = A(1 - u_n)u_n, \tag{2.5}$$

where $u = (ab/1+a)x$ and $A = 1+a$. We denote $f(u_n)$ the right-hand side of (2.5). We assume that the domain of x is $[0,1]$. For $0 \leq A \leq 4$, the range of the logistic map f is included in $[0,1]$. We can construct the solution of (2.5) by a diagram method (see Fig. 2.1).

By changing A, we observe different behavior of the solution. For $0 < A \leq 1$, the parabolic curve and the line in the diagram do not intersect in the domain of u, and hence, we observe $\lim_{n\to\infty} u_n = 0$. For $1 < A \leq 4$, we obtain the intersection, which represents the fixed point of the logistic map. As far as this fixed point appears in the range of $u < 1/2$ $(1 < A \leq 2)$, it is stable, so that u_n converges to it. In the range of $2 < A \leq 4$, u_n oscillates around the fixed point. For $3 < a \leq 4$, the fixed point becomes unstable. However, the double-period map $f^2(u_n) = f(f(u_n))$ has a stable fixed point for a slightly larger A than f. The quadra-period map $f^4(u_n)$ has a more large range of A. Therefore, by increasing A, we obtain period-doubling bifurcations. It is known, however, the period diverges around $A = 3.57$, and beyond this critical value, the sequence u_n does not have any periodicity. This infinite-period oscillation is called "chaos".

By comparing the continuous model (2.2) and the discrete model (2.4), we find that the nonlinearity behaves very differently under a slight modification. We never observe such a drastic difference when we discretize the linear model (2.1).

The discretization may introduce a slight destablizing effect. By the competition of the instability and the fundamental stability of the system (as shown in (2.3), the discrete logistic model produces chaos.

2.2 Carleman embedding

Let us consider a simplified version of the continuous logistic model (2.2);

$$\frac{d}{dt}u = -u + u^2, \tag{2.6}$$

and introduce the following "linearization" method. We write

$$y_1 = u, \quad y_2 = u^2, \quad y_3 = u^3, \quad \cdots. \tag{2.7}$$

By the definition, we observe

$$\frac{dy_n}{dt} = nu^{n-1}\frac{du}{dt}.$$

Using (2.6), we obtain

$$\frac{d}{dt}y_n = -ny_n + ny_{n+1} \quad (n = 1, 2, \cdots). \tag{2.8}$$

If we consider the infinite number of variables $y_1, y_2, \cdots$ as independent variables, (2.8) reads as a system of infinite-dimension linear ordinary differential equations (ODEs)

$$\frac{d}{dt}\begin{pmatrix} y_1 \\ y_2 \\ y_3 \\ \vdots \end{pmatrix} = \begin{pmatrix} -1 & 1 & 0 & \cdots & & \\ 0 & -2 & 2 & 0 & \cdots & \\ 0 & 0 & -3 & 3 & 0 & \cdots \\ & & & \ddots & \ddots & \end{pmatrix} \begin{pmatrix} y_1 \\ y_2 \\ y_3 \\ \vdots \end{pmatrix}. \tag{2.9}$$

The nonlinear ODE (2.6), obeyed by u, and the system of linear ODEs (2.9), obeyed by $y_1, y_2, \cdots$ are equivalent under the condition (2.7). To put it in a more precise way, let $u(t)$ be a solution of (2.6) with the initial condition $u(0) = c$ $(0 \leq c \leq 1)$. By (2.7), we can define $y_n(t)$ $(n = 1, 2, \cdots)$. Then, these $y_n(t)$ satisfy (2.9) and the initial condition

$$y_n(0) = c^n \quad (n = 1, 2, \cdots). \tag{2.10}$$

On the centrally, if we could solve (2.9) under the initial condition (2.10), and if they satisfy $y_j = y_1^j$ $(j = 2, 3, \cdots)$, [2] the first component $y_1(t) = u(t)$ solves (2.6). We call this technical linearization as "Carleman embedding" [8].

Note 3 (Fock space) *Let us consider a nonlinear ODE obeyed by a vector variable $\boldsymbol{u} \in \mathbf{R}^N$. We assume that the nonlinear term is given by polynomials. We denote tensor products*

$$\boldsymbol{u}^{(1)} = \boldsymbol{u}, \quad \boldsymbol{u}^{(2)} = \boldsymbol{u} \otimes \boldsymbol{u}, \quad \boldsymbol{u}^{(3)} = \boldsymbol{u} \otimes \boldsymbol{u} \otimes \boldsymbol{u}, \quad \cdots.$$

The linear space of j tensors is denote by $\bigotimes^j \mathbf{R}^N$. Let A_j be a linear map of $\bigotimes^j \mathbf{R}^N \to \mathbf{R}^N$. If the highest order of the nonlinear term is k, the general form of ODEs can be written as

$$\frac{d}{dt}\boldsymbol{u} = A_0 + A_1\boldsymbol{u} + \cdots + A_k\boldsymbol{u}^{(k)}. \tag{2.11}$$

Denoting $y_j = \boldsymbol{u}^{(j)}$, we consider an infinite-dimension vector variable $y =^t (y_1, y_2, \cdots)$, which is a member of a "Fock space"

$$F = \bigoplus_{j=1}^{\infty} \bigotimes^j \mathbf{R}^N,$$

where $\bigoplus$ is the direct sum of linear spaces. The solution of the nonlinear ODEs (2.11) can be embedded in the solution of the linear ODEs in the Fock space F.

Mathematical justification for the above-mentioned infinite-dimension linear ODEs must be carefully done, since the coefficient matrix contains unbounded elements. Let us solve (2.9) explicitly. We appeal to the Laplace transform. Let us define

$$\hat{y}_n(s) = \int_0^\infty e^{-st} y_n(t) dt \quad (s \in \boldsymbol{C}). \tag{2.12}$$

[2] (2.9) has non-unique solutions that do not satisfy this condition

We assume that, for some real number s_0 and Re $s > s_0$, the integral of (2.12) converges. Integrating by parts yields

$$\int_0^\infty e^{-st}\frac{dy_n}{dt}dt = s\hat{y}_n(s) - y_n(0).$$

Using this relation in (2.9), and using the initial condition (2.10), we obtain

$$(n+s)\hat{y}_n(s) - n\hat{y}_{n+1}(s) = c^n \quad (n = 1, 2, \cdots).$$

We can solve this equation sequentially as

$$\hat{y}_1(s) = \frac{c}{1+s} + \frac{c^2}{(1+s)(2+s)} + \frac{2c^3}{(1+s)(2+s)(3+s)} + \cdots$$

$$= \sum_{n=1}^{\infty} \frac{\Gamma(n)\Gamma(s+1)c^n}{\Gamma(n+s+1)} = \sum_{n=1}^{\infty} c^n B(n, s+1), \tag{2.13}$$

where Γ is the Gamma function and B is the Beta function. By the identity

$$B(p,q) \equiv \frac{\Gamma(p)\Gamma(q)}{\Gamma(p+q)} = \int_0^1 x^{p-1}(1-x)^{q-1}dx \quad (\text{Re } p, \text{Re } q > 0),$$

and (2.13), we obtain

$$\hat{y}_1(s) = \int_0^1 (1-cx)^{-1}(1-x)^s dx. \tag{2.14}$$

Transforming $(1-x) = e^{-t}$, (2.14) reads

$$\hat{y}_1(s) = \int_0^\infty e^{-st}\frac{c}{c+(1-c)e^t}dt.$$

Comparing the definition (2.12), we now obtain

$$y_1(t) = \frac{c}{c+(1-c)e^t}.$$

As we have shown in the previous section, the continuous logistic model (2.6) is very close to a linear category. If we consider a truly nonlinear system that produces chaos, we meet the following problem, that reveals the origin of complexity. Let us consider an abstract nonlinear autonomous system. Let us denote by $\mathcal{L}$ the infinite-dimension matrix that is embedding the nonlinear dynamics. We formally write the eigenvalues of $\mathcal{L}$ as λ_j $(j = 1, 2, \cdots)$, each of which represents a time constant of the infinite-dimension system. If Re $\lambda_j \leq M$ $(\forall\lambda_j)$ for some real number M, the infinite dimension system can be solved by the Laplace transform, and we can estimate

$$|y_j(t)| \leq C_j e^{tM} \quad (j = 1, 2, \cdots), \tag{2.15}$$

where C_j is a constant determined by the initial condition. For the continuous logistic model, the eigenvalues of the generator in (2.9) is given by $\lambda_j = -j$ $(j = 1, 2, \cdots)$, and hence, the

above-mentioned condition is satisfied. However, if $\{\mathrm{Re}\ \lambda_j;\ j = 1,2,\cdots\}$ is unbounded in the positive direction, the general solution contains infinitely large growth rates. Roughly speaking, when the maximum Lyapunov exponent of $u(t)$ is Λ, then $u^{(n)}(t)$ has the maximum Lyapunov exponent of order $n\Lambda$. If $u(t)^{(n)}$ is embedded in $y(t)$, (2.15) implies that there exist eigenvalues that have larger real parts than $n\Lambda$. A chaotic orbit $u(t)$ has $\Lambda > 0$, and hence $\{\mathrm{Re}\ \lambda_j;\ j = 1,2,\cdots\}$ is unbounded. In this case the chaotic solution $y(t) =^t (u(t), u^{(2)}(t), \cdots)$ exists as a special solution of the linearized equation, while its general solution cannot be generated by the evolution equation.

This situation is similar to the "inverse" diffusion equation;

$$\partial_t u = -\partial_x^2 u, \quad u(x,0) = u_0,\ u(0,t) = u(\pi,t) = 0.$$

By Fourier transforming $u(x,t) = \sum_j u_j(t)\sin(jx)$, we obtain

$$\frac{d}{dt}\begin{pmatrix} u_1 \\ u_2 \\ u_3 \\ \vdots \end{pmatrix} = \begin{pmatrix} 1\,0\,0\cdots & & \\ 0\,4\,0\ \ 0\ \cdots & & \\ 0\,0\,9\ \ 0\ \ 0\ \cdots & & \\ \ddots\ \ddots & & \end{pmatrix}\begin{pmatrix} u_1 \\ u_2 \\ u_3 \\ \vdots \end{pmatrix}. \tag{2.16}$$

This "ill-posed" problem cannot be solved uniquely, while it has special solutions. The fundamental difference between the Carleman-linearized system and the linear system (2.16) is that "mode interactions" (i.e., off-diagonal components in the generator matrix) does not occur in the linear system.

2.3 Example III (chaotic oscillation of magnetic filed)

2.3.1 MHD equations and Beltrami condition

The nonlinear magnetohydrodynamics (MHD) involves a variety of complex phenomena. It is impossible to construct nontrivial theory by direct analyses of the basic equations. To elucidate a specific phenomenon, we must apply a reduction of the model with appealing to scale separations, singular perturbations, coarse-graining (averaging), etc.

In this section, we discuss a slow motion (or a steady state) of a low-pressure magnetized plasma. In more specific terms, we consider the following singular limit. The general MHD equations read, in the standard normalized units,

$$\partial_t \boldsymbol{v} = -(\boldsymbol{v}\cdot\nabla)\boldsymbol{v} + \epsilon_A^{-2}(\nabla\times\boldsymbol{B})\times\boldsymbol{B} - \beta\nabla p + \epsilon_R\Delta\boldsymbol{v}, \quad \nabla\cdot\boldsymbol{v} = 0, \tag{2.17}$$

$$\partial_t \boldsymbol{B} = \nabla\times(\boldsymbol{v}\times\boldsymbol{B}) - \epsilon_L\nabla\times(\nabla\times\boldsymbol{B}). \tag{2.18}$$

Unknown variables are the magnetic field $\boldsymbol{B}$, the flow velocity $\boldsymbol{v}$ and the pressure p. The Alfvén number ϵ_A, Lundquist number ϵ_L^{-1}, Reynolds number ϵ_R^{-1}, and the beta ratio β are nondimensional positive parameters. The incompressibility condition ($\nabla\cdot\boldsymbol{v} = 0$) may be replaced by an evolution equation for the pressure p in a more sophisticated model.

This system of nonlinear parabolic equations (2.17)–(2.18) is a close cousin of the Navier-Stokes system describing neutral fluids (see [9, 19] and papers cited therein). The MHD system includes coupling between the magnetic field and the flow velocity through the nonlinear induction effect and its reciprocal Lorentz force, which adds a considerable complexity to the usual Navier-Stokes system. Surprisingly, however, we observe a more regular and ordered behavior in some MHD systems. Such phenomena are highlighted by a singular perturbation of $\epsilon_A^2 \to 0$, with fixing the time-scale, in the momentum-balance equation (2.17). This limit is amenable to slow motion of a strongly magnetized low β plasma. The determining equation becomes the force-free condition $(\nabla \times \boldsymbol{B}) \times \boldsymbol{B} = 0$, which is equivalent to the Beltrami condition

$$\nabla \times \boldsymbol{B} = \lambda \boldsymbol{B}. \tag{2.19}$$

Here λ is a scalar function. By the solenoidal condition ($\nabla \cdot \boldsymbol{B} = 0$) and identity $\nabla \cdot (\nabla \times \boldsymbol{B}) = 0$, taking the divergence of the both sides of (2.19) yields

$$\boldsymbol{B} \cdot \nabla \lambda = 0. \tag{2.20}$$

Since (2.20) means that the function λ should be constant along the streamline (field line) of $\boldsymbol{B}$, analysis of the system of equations (2.19)–(2.20) requires integration of the streamline equation

$$\frac{d}{d\tau}\boldsymbol{x} = \boldsymbol{B}(\boldsymbol{x}). \tag{2.21}$$

The solenoidal condition ($\nabla \cdot \boldsymbol{B} = 0$) parallels Liouville's theorem for the Hamiltonian flow, and one can formulate (2.21) in a canonical form (see Note 2). For a general three-dimensional $\boldsymbol{B}$, the solution of (2.21) exhibits chaos (Sec. 1.3). Hence, the general analysis of the system (2.19)–(2.20) includes an essential mathematical difficulty. Two special cases, however, can be studied rigorously. One is the case where $\boldsymbol{B}$ has an ignorable coordinate (two-dimensional). Then, (2.21) becomes integrable, and the system (2.19)–(2.20) reduces into a nonlinear elliptic equation [3, 24]. The three-dimensional problem involves the non-integrable streamline problem (2.21), however, it is decoupled from the Beltrami problem (2.19)–(2.20), if we assume a constant λ that make (2.20) trivial. This "constant-λ beltrami field" will be discussed in Sec. 3.5.

2.3.2 Reduced model of interacting magnetic islands

In this section, we consider nonlinear interactions among plasma elements with inhomogeneous λ. Each element satisfies the constant-λ Beltrami condition (2.19). Different elements are separated by a thin layer where the magnetic field lines are weakly chaotic. Hence, the connection lengths among different elements are considerably long. If we consider a small deviation from the Beltrami condition (2.19), and write

$$\nabla \times \boldsymbol{B} = \lambda \boldsymbol{B} + \boldsymbol{\alpha}, \tag{2.22}$$

then (2.20) receives a small correction and becomes

$$(\boldsymbol{B} \cdot \nabla)\lambda = -\nabla \cdot \boldsymbol{\alpha}. \tag{2.23}$$

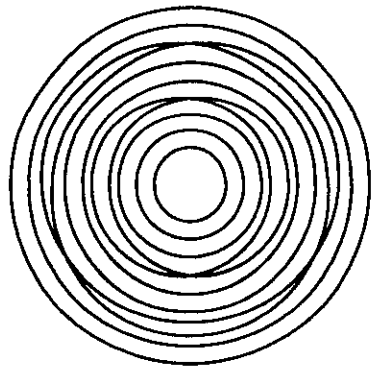

Figure 2.2: Magnetic-field perturbations induced by resistive instabilities (tearing modes) change the field-line structure in a tokamak plasma to generate magnetic islands, and their overlapping leads to magnetic chaos.

Integrating (2.23) along a field line, we obtain a finite inhomogeneity in λ after a long distance. This allows us to assume inhomogeneous λ in the following discussion. We consider a cylindrical plasma with radial inhomogeneity.

We introduce a reduced ODE system that models nonlinear interactions of magnetic islands produced by the tearing instability (see fig. 2.2). The basic idea of the reduction is the use of the Beltrami condition ($\nabla \times \boldsymbol{B} = \lambda \boldsymbol{B}$) to convert the spatial derivatives in the PDE system (2.17)–(2.18) into the multiplying of λ. We note that this procedure differs from the Fourier decomposition and truncation, which are usually used to derive reduced models in different problems. For each mode of Fourier decomposition, we can replace derivatives by multiplying of wavenumbers. In the present method, the conversion applies to the exact function, not to expansion modes. The λ is a dynamical variable to be determined by the evolutions equation. Here we invoke a quasilinear turbulence model of MHD fluctuations (see [1, 13, 22] and papers cited therein).

Magnetic field $\boldsymbol{B}$ is decomposed into the fluctuating component $\boldsymbol{b}$ and the ambient component $\boldsymbol{B}_0$. For the plasma velocity $\boldsymbol{v}$, we also assume two components; One the a uniform flow $\boldsymbol{V}$ and the other is the fluctuation $\tilde{\boldsymbol{v}}$ driven by the MHD instabilities. Assuming a quasilinear turbulence of resistive instabilities, we may write the ensemble average of the nonlinear term $\langle \tilde{\boldsymbol{v}} \times \boldsymbol{b} \rangle$ in terms of the growth rate of the instability, the energy of fluctuations, and some geometric factors. The parallel (with respect to the mean magnetic field $\boldsymbol{B}_0$) component of $\langle \tilde{\boldsymbol{v}} \times \boldsymbol{b} \rangle$ makes an essential contribution, which is denoted by $-E_{\|}^{(2)}$. The quasilinear turbulence theory [13] yields

$$E_{\|}^{(2)} = -\nabla \cdot (\eta^{(2)} \nabla j_{\|,0}),$$

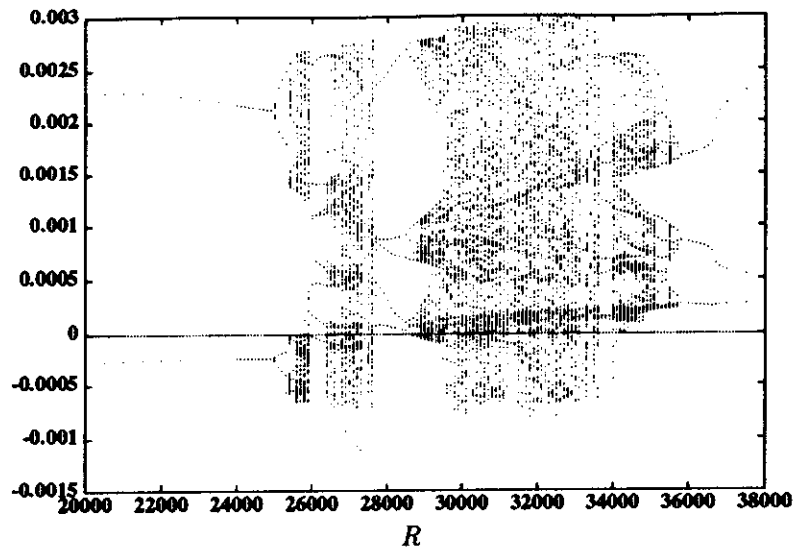

Figure 2.3: Feigenbaum diagram for R in the range of $2.0 \times 10^4 - 3.8 \times 10^4$.

where $\eta^{(2)}$ is the *hyper resistivity* given by

$$\frac{\eta^{(2)}}{\mu_0} = \frac{1}{2}\sum_k \frac{\gamma_k}{(\partial_r k_{||})^2}|b_{r,k}|^2 \ln\left(\frac{r_k^2}{(r-r_k)^2 + \gamma_k^2/(\partial_r k_{||})^2}\right). \tag{2.24}$$

Here the subscript k indicates a Fourier component of the fluctuation, γ_k is the growth rate and $k_{||}$ is the parallel wavenumber with $k_{||}(r_k) = 0$. The ensemble average of Faraday's law (2.18) becomes

$$\partial_t \boldsymbol{b} = -\epsilon_L \nabla \times (\nabla \times \boldsymbol{b}) + \nabla \times (\boldsymbol{V} \times \boldsymbol{b} - E_{||}^{(2)} \nabla z). \tag{2.25}$$

We assume $\boldsymbol{B}_0 = \nabla z$. The Beltrami condition reads $\nabla \times \boldsymbol{b} = \lambda(\boldsymbol{b} + \boldsymbol{B}_0)$. We obtain

$$\nabla \times (\nabla \times \boldsymbol{b}) = \lambda^2 \boldsymbol{b} + \nabla\lambda \times (\boldsymbol{b} + \boldsymbol{B}_0),$$

$$\nabla \times (\boldsymbol{V} \times \boldsymbol{b}) \approx -(\nabla \times \boldsymbol{b}) \times \boldsymbol{V} = -\lambda \boldsymbol{b} \times \boldsymbol{V}.$$

We consider a low pressure plasma, so that the parallel component of $\boldsymbol{b}$ is neglected. In the cylindrical coordinates such that $\nabla\varphi \times \nabla r = \nabla z$ (φ and r are the angle and radial coordinates, respectively), we write $p = b_r$ and $q = b_\varphi$. Inhomogeneity of the plasma is assumed in the direction of ∇r. We may write the φ and r components of (2.25) as

$$\partial_t p = -\epsilon_L \lambda^2 p - V\lambda q, \tag{2.26}$$

$$\partial_t q = -\epsilon_L \lambda^2 q + V\lambda p - \partial_r E_{||}^{(2)} \tag{2.27}$$

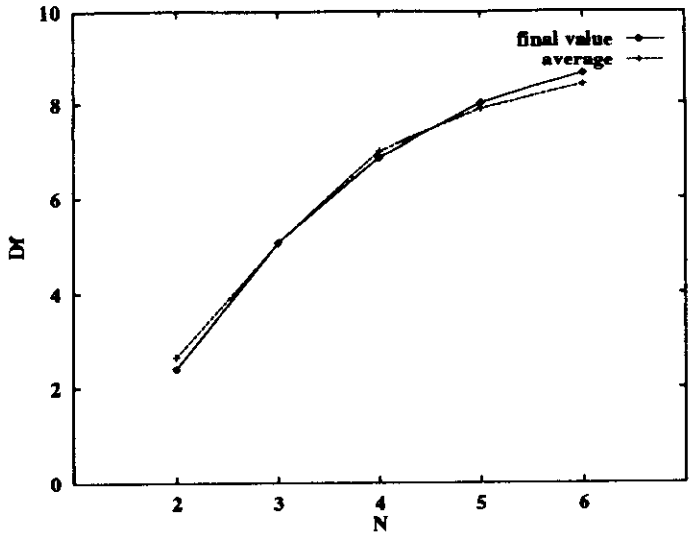

Figure 2.4: Dependence of the Lyapunov dimension on N.

The last term in the right hand side of equation (2.27) represents the effect of the MHD fluctuations. We can write

$$\frac{\partial E_{\parallel}^{(2)}}{\partial r} = -\frac{2}{\mu_0}\frac{\partial \eta^{(2)}}{\partial r}\frac{\partial^2 \lambda}{\partial r^2}.$$

Two unknown variables p and q represent the amplitude of the magnetic perturbation $\boldsymbol{b}$. The third unknown variable λ characterizes the "curl" of $\boldsymbol{b}$. The equation obeyed by λ, which is also derived from (2.25), becomes [22]

$$\partial_t \lambda = C\langle p\rangle^2 \lambda^2 \frac{\partial^2 \lambda}{\partial r^2} + E_h \lambda^2,$$

where E_h is the external driving electric field.

We note that the factor $\partial^2\lambda/\partial r^2$ represents the diffusion of the helicity induced by the MHD fluctuations. We discretize the radial coordinate into points where some different instabilities are resonant. Replacing the spatial derivatives of the helicity diffusion by difference quotients, we obtain the reduced model equations

$$\dot{p}_n = -\epsilon_L \lambda_n^2 p_n - V\lambda_n q_n, \tag{2.28}$$

$$\dot{q}_n = -\epsilon_L \lambda_n^2 q_n + V\lambda_n p_n + Q_n(p_{n-1}, p_{n+1}, \lambda_{n-1}, \lambda_n, \lambda_{n+1}), \tag{2.29}$$

$$\dot{\lambda}_n = \lambda_n^2 \left(L_n(p_n, \lambda_{n-1}, \lambda_n, \lambda_{n+1}) + E_h\right), \tag{2.30}$$

where n $(= 1, 2, \cdots N)$ indicates the n^{th} radial position,

$$Q_n(p_{n-1}, p_{n+1}, \lambda_{n-1}, \lambda_n, \lambda_{n+1}) = 2C \frac{\langle p_{n+1} \rangle^2 - \langle p_{n-1} \rangle^2}{\Delta} \frac{\lambda_{n+1} + \lambda_{n-1} - 2\lambda_n}{\Delta^2},$$

$$L_n(p_n, \lambda_{n-1}, \lambda_n, \lambda_{n+1}) = C \langle p_n \rangle^2 \frac{\lambda_{n+1} + \lambda_{n-1} - 2\lambda_n}{\Delta^2},$$

Δ is a radial distance between the radial grid points, and N is the number of interacting islands with different helicities.

2.3.3 Lyapunov dimension

The model equations (2.28)-(2.30) generate chaotic orbits of the solution. The typical parameters are

$$\lambda = 10^{-1} \sim 1, \quad |p|, |q| = 10^{-4} \sim 10^{-2}, \quad \epsilon_L = 10^{-6} \sim 10^{-5},$$

$$C = 10^{-1} \sim 1, \quad \Delta \sim 10^{-1}, \quad V = 10^{-5} \sim 10^{-3}, \quad E_h = 10^{-8} \sim 10^{-7}.$$

Changing the Lundquist number $R = \epsilon_L^{-1}$ (magnetic Reynolds number), we observe bifurcation and inverse cascade in the chaotic behavior of the solution. Figure 2.3 shows the Feigenbaum diagram, where we plot peak points of the time series with changing R. Here we fix other parameters as $N = 3$, $C = 1.0$, $\Delta = 0.1$, $V = 7.72 \times 10^{-5}$ and $E_h = 1.0 \times 10^{-8}$. We observe two branches bifurcate into chaos. For a larger R, the chaos quenches and periodic attractor appears.

The total number N of modes defines the freedom of the model equations, which is $3 \times N$. Figure 2.4 shows the dependence of Lyapunov dimension D_f on N.

Chapter 3

Complexity

3.1 Mixing

Mixing induced by inhomogeneous flow is one of the central paradigms of generating complexity. When an inhomogeneous flow transports a physical quantity, the spatial variation of its distribution is enhanced. This process acts also to homogenize distributions of physical quantities in a "coarse-grained" sense. When we mix milk in coffee using a spoon, we intend to smooth out the density of milk, but not to create complex distribution. These two different aspects, the creation and annihilation of complexity, are the simultaneous characteristics of complex systems, i.e., complex systems show different faces depending on our view points.

We start with a simple model of mixing process that simulates baker's work of making a pie. Let ϕ be a transform

$$\begin{pmatrix} x_{n+1} \\ y_{n+1} \end{pmatrix} = \phi \begin{pmatrix} x_n \\ y_n \end{pmatrix} = \begin{cases} \begin{pmatrix} 2x_n \\ \frac{1}{2}y_n \end{pmatrix} & (0 \le x_n \le \frac{1}{2}) \\ \\ \begin{pmatrix} 2x_n - 1 \\ \frac{1}{2}(y_n + 1) \end{pmatrix} & (\frac{1}{2} \le x_n \le 1) \end{cases}, \tag{3.1}$$

which maps a rectangular domain $\Omega = \{(x, y);\ 0 \le x \le 1, 0 \le y \le 1\}$ into Ω itself. Figure 3.1 illustrates this map.

By applying the transform of x, y induced by ϕ, we define a transform of a distribution $f_n(x, y)$ that is continuous function of Ω;

$$f_{n+1}(x, y) = f_n(\phi^{-1}(x, y)) = \begin{cases} f_n(\frac{1}{2}x, 2y) & (0 \le y \le \frac{1}{2}) \\ \\ f_n(\frac{1}{2}(x + 1), 2y - 1) & (\frac{1}{2} \le y \le 1) \end{cases}. \tag{3.2}$$

After many application of this transform, $f_n(x, y)$ becomes to have a strong inhomogeneity in y-direction (Fig. 3.1). Since we bite a pie in the vertical direction, let us integrate $f_n(x, y)$ with respect to y;

$$g_n(x) = \int_0^1 f_n(x, y)dy. \tag{3.3}$$

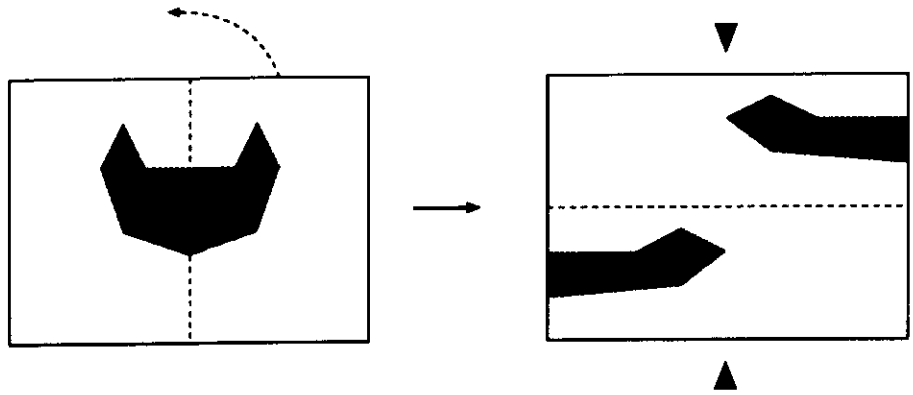

Figure 3.1: Baker's transform.

This "integral" introduces a "coarse-graining". By the definition, we observe

$$g_{n+1}(x) = \int_0^{1/2} f_n(\frac{1}{2}x, 2y)dy + \int_0^{1/2} f_n(\frac{1}{2}(x+1), 2y-1)dy$$

$$= \frac{1}{2}\left[g_n(\frac{1}{2}x) + g_n(\frac{1}{2}(x+1))\right]. \tag{3.4}$$

This process yields averaging of the left and right sides of the center $x = 1/2$, and hence, $g_n(x)$ converges into a homogeneous distribution at the limit of $n \to \infty$.

By this simple example, we have seen that Baker's transform (3.1) induces mixing in the x-y plane, and it produces complex distributions in y-direction. However, the coarse-grained distribution $g_n(x)$ relaxes into a homogeneous distribution. We notice that the transform (3.2) of the detailed distribution $f_n(x, y)$ is temporally-reversible (we can calculate $f_n \to f_{n-1}$ uniquely), while the transform (3.4) of the coarse-grained distribution $g_n(x)$ is no longer reversible. This irreversibility is introduced by the loss of information associated with the coarse-graining. As long as retaining the microscopic detailed data, we can backtrack the process. Throwing away unnecessary details, we obtain a more sensible description of a complex system, but this introduces irreversibility.

3.2 Convection and induction

In this section, we give a formal representation of mixing induced by a flow. We consider a flow $\boldsymbol{v}$ in a domain (phase space) $\Omega \subset \mathbf{R}^N$. Let $\boldsymbol{v}$ be a smooth function of time t and position $\boldsymbol{x}$ ($\in \Omega$). We can define the "streamline" by solving the following initial value problem of

ordinary differential equation

$$\frac{d\boldsymbol{x}}{dt} = \boldsymbol{v}(\boldsymbol{x}, t). \tag{3.5}$$

In terms of geometry, the streamline is a curve whose tangent vector is $\boldsymbol{v}$. The time t is a parameter indicating the position on the curve (cf. Sec. 1.3).

We consider a physical quantity u that is a smooth function of t and $\boldsymbol{x}$ ($\in \Omega$). In evaluating u on the streamline $\boldsymbol{x}(t)$, that is a solution of (3.5), the temporal derivative along the streamline becomes

$$\frac{d}{dt}u(\boldsymbol{x}(t), t) = \partial_t u + (\boldsymbol{v} \cdot \nabla)u.$$

If u is constant through every streamline, viz., if u is a conserved quantity associated with the phase-space dynamics $\boldsymbol{v}$, this u must satisfy the "transport equation"

$$\partial_t u + (\boldsymbol{v} \cdot \nabla)u = 0. \tag{3.6}$$

This partial differential equation (PDE) has a wave-type solution that represents the propagation of the variation of u induced by the flow $\boldsymbol{v}$. In mathematical terms, the streamlines correspond to the "characteristic curves" of the hyperbolic PDE (3.6). When the streamline equations are written in a canonical form, the study of the characteristic curves parallels the Hamiltonian dynamical system theory.

Note 4 (Hamiltonian flow and Liouville's equation) *Incompressible flow is of particular importance. The streamline of incompressible flow does not break out or disappear, and hence, defines an isomorphic transformation group. The most important class of incompressible flow is the Hamiltonian flow. Let $\boldsymbol{x}$ and $\boldsymbol{y}$ denote the canonical coordinate and momentum, respectively. Hamilton's equation of motion reads*

$$\frac{d}{dt}\begin{pmatrix}\boldsymbol{x}\\ \boldsymbol{y}\end{pmatrix} = \begin{pmatrix}\partial_{\boldsymbol{y}}\mathcal{H}\\ -\partial_{\boldsymbol{x}}\mathcal{H}\end{pmatrix}, \tag{3.7}$$

where $\mathcal{H}$ is the Hamiltonian. We denote by $\partial_{\boldsymbol{x}}$ and $\partial_{\boldsymbol{y}}$ the gradients with respect to $\boldsymbol{x}$ and $\boldsymbol{y}$, respectively. Writing

$$\boldsymbol{X} = \begin{pmatrix}\boldsymbol{x}\\ \boldsymbol{y}\end{pmatrix}, \quad \boldsymbol{V} = \begin{pmatrix}\partial_{\boldsymbol{y}}\mathcal{H}\\ -\partial_{\boldsymbol{x}}\mathcal{H}\end{pmatrix}, \tag{3.8}$$

we observe that (3.7) is just the streamline equation (3.5) in the phase space $\boldsymbol{x}$-$\boldsymbol{y}$. In this space, the divergence of the Hamiltonian flow is calculated as

$$\nabla \cdot \boldsymbol{V} = \sum \partial_{x_j}\partial_{y_j}\mathcal{H} - \sum \partial_{y_j}\partial_{x_j}\mathcal{H} = 0.$$

Therefore, the Hamiltonian flow $\boldsymbol{V}$ is incompressible in the phase space (Liouville's theorem). The convective derivatives of $u(\boldsymbol{x}, \boldsymbol{y}, t)$ becomes

$$\partial_t u + (\boldsymbol{V} \cdot \nabla)u = \partial_t u + \{\mathcal{H}, u\}, \tag{3.9}$$

where, by (3.8),

$$\{\mathcal{H}, u\} \equiv (\partial_{\boldsymbol{y}}\mathcal{H}) \cdot (\partial_{\boldsymbol{x}} u) - (\partial_{\boldsymbol{x}}\mathcal{H}) \cdot (\partial_{\boldsymbol{y}} u).$$

We call the bilinear operator $\{,\}$ the Poisson bracket. If u is a constant of motion, Liouville's equation holds:

$$\partial_t u + \{\mathcal{H}, u\} = 0. \tag{3.10}$$

We have shown that the canonical form of the convective derivative is represented by the Poisson bracket.

The simplest model of fluid mechanics is the Euler equation, which describes the acceleration of an ideal incompressible fluid by a pressure (potential force). We assume that the mass density of the fluid is 1. The "inertia force" is evaluated by calculating the temporal variation of the flow $\boldsymbol{v}$ along the streamline. Equating the inertia force and the pressure, we obtain the Euler equation

$$\partial_t \boldsymbol{v} + (\boldsymbol{v} \cdot \nabla)\boldsymbol{v} = -\nabla p, \quad \nabla \cdot \boldsymbol{v} = 0. \tag{3.11}$$

Calculating the curl of the first equation of (3.11), we obtain the "vortex equation"

$$\partial_t \boldsymbol{w} - \nabla \times (\boldsymbol{v} \times \boldsymbol{w}) = 0, \tag{3.12}$$

where $\boldsymbol{w} \equiv \nabla \times \boldsymbol{v}$ is the vorticity of the flow.

In (3.11), the spatial derivatives appear in the form of the convective derivative $(\boldsymbol{v} \cdot \nabla)$, while, in (3.12), they take a different form $-\nabla \times (\boldsymbol{v} \times\ )$. We call this second type of derivative as an "induction". This induction is a close cousin of the convection. In fact, using vector identities, we observe

$$-\nabla \times (\boldsymbol{v} \times \boldsymbol{w}) = (\boldsymbol{v} \cdot \nabla)\boldsymbol{w} - (\boldsymbol{w} \cdot \nabla)\boldsymbol{v}. \tag{3.13}$$

The first term in the right-hand side of (3.13) is nothing but the convective derivative of the vorticity. The second term plays an essential role in the discussion of nonlinear behavior of fluids and plasmas. Here, we note that this second term disappears in the case of two dimension ($N = 2$), and hence, for a two-dimensional system, the convection and induction are not distinguished. A two dimensional flow is embedded in a three dimensional flow (we consider x-y-z cartesian system) by assuming $\partial_z = 0$ and $v_z = 0$. We observe

$$\boldsymbol{w} = w_z \boldsymbol{e}_z, \quad (\boldsymbol{w} \cdot \nabla) = w_z \partial_z \equiv 0.$$

Hence, in two-dimension system, $-\nabla \times (\boldsymbol{v} \times \boldsymbol{w}) = (\boldsymbol{v} \cdot \nabla)\boldsymbol{w}$.

Let us give another important example of the induction. If we consider a perfectly conducting fluid (plasma), the electric field in the fluid must vanish. When the fluid moves in a magnetic field $\boldsymbol{B}$, the vanishing of the electric field in the fluid is represented in terms of the electric field $\boldsymbol{E}$ and the velocity $\boldsymbol{v}$, that are evaluated in the laboratory frame, by

$$\boldsymbol{E} + \boldsymbol{v} \times \boldsymbol{B} = 0. \tag{3.14}$$

Using the Faraday's law $\partial_t \boldsymbol{B} = -\nabla \times \boldsymbol{E}$, and taking the curl of the both sides of (3.14), we obtain

$$\partial_t \boldsymbol{B} - \nabla \times (\boldsymbol{v} \times \boldsymbol{B}) = 0. \tag{3.15}$$

We note the analogy of this "induction equation" and the vortex equation (3.12).

3.3 Linear theory of mixing – Landau damping

We now proceed to show a very simple example of a low-dimensional dynamics that can generate appreciable complexity. We would also show how a very innocent-looking coarse-graining procedure can introduce irreversibility. The system to be studied is so simple that we need to invoke neither a statistical model, nor collisions to create irreversibility.

Complexity, however, develops in the system, because all particles are un-correlated.

Consider a set of "independent" particles that move with constant velocities (v) in one dimensional space. The relevant phase space x-v is two dimensional. The phase space density or the distribution function $f(x,v,t)$ obeys the Liouville equation (3.10)

$$\partial_t f + v\partial_x f = 0, \tag{3.16}$$

which allows the D'Alembert solution

$$f(x,v,t) = f_0(x - vt, v), \tag{3.17}$$

where $f_0(x,v)$ is the initial distribution of f. For $f_0(x,v)$, let us assume, as an example, a Maxwell-Boltzmann distribution in energy E ($= v^2/2$ for particles of unit mass), and a sinusoidal wave (on a constant background) in x;

$$f_0(x,v) = \left(A + ae^{ikx}\right) e^{-v^2/v_T^2}.$$

Here, A, a and v_T (thermal velocity) are constants. For this initial condition, (3.17)yields

$$f(x,v,t) = \left(A + ae^{ik(x-vt)}\right) e^{-v^2/v_T^2}. \tag{3.18}$$

For a fixed v, this solution represents a free wave propagating at a constant velocity v. If different particle have different velocities, the distribution of f in the x-v space becomes complicated. In order to obtain some kind of a representative picture, we "coarse-grain" the structure in v by integrating over v , and obtain the coordinate-space density

$$n(x,t) = \int_{-\infty}^{\infty} f(x,v,t)dv = \sqrt{2\pi}Av_T + ae^{ikx}\int_{-\infty}^{\infty} e^{-ikvt}e^{-v^2/v_T^2}dv$$

$$= \sqrt{\pi}Av_T + \sqrt{\pi}av_T^2 e^{ikx}e^{-k^2v_T^2t^2/4}.$$

The factor $e^{-k^2v_T^2t^2/4}$ decays to zero as $t \to \infty$, and hence the macroscopic quantity $n(x,t)$ relaxes into a flat distribution $\sqrt{2\pi}Av_T$.

The cause of the above-mentioned relaxation is the *mixing* induced by the inhomogeneous flow in phase space (Fig. 3.2). The instrument we used to "mix" was the integration in the velocity space. Note that before mixing , the phase space density f consisted of a set of waves merrily propagating with a distribution of velocities. If the particle motions were correlated, for example, if we used a delta function as the velocity distribution (instead of the Maxwellian), the v integration will do next to nothing (no mixing), and the coordinate-space density will also

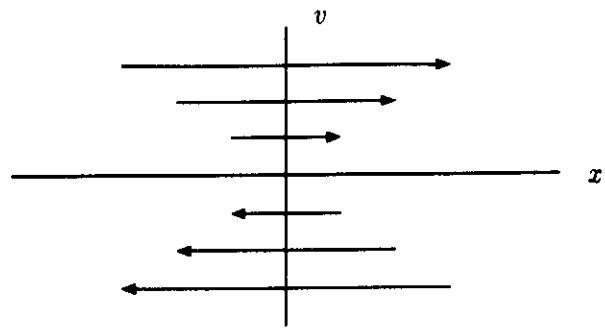

Figure 3.2: Phase-space flow representing free particle motion. This sheared flow in velocity space induces mixing. The coarse-graining (averaging) over v results in relaxation.

turn out to be a wave propagating with the common velocity of the particles. There will be no relaxation, then! Thus the possibility of relaxation, or irreversibility was created entirely by destroying the individual uncorrelated memories by churning (by integration) them together.

The collision-less mechanism of relaxation is a profound many-body effect, that is the central issue of the "Landau damping" of collective motion (waves) in plasmas. It plays a fundamental role in the understanding of collective phenomena in plasmas, and gravitational many-body systems.

Let us show the mixing damping of a wave is a characteristic of "continuous spectrum". We consider a linear convective equation (Liouville equation)

$$\partial_t f + y\partial_x f = 0. \tag{3.19}$$

Here $x \in \mathbf{R}$ represents the position and $y \in \mathbf{R}$ represents the velocity (momentum), and $f(x, y, t)$ is the distribution function, which is assume to be in $L^2(\mathbf{R})$.

Fourier transform f with respect to x, and write $\hat{f}(k, y, t) = \mathcal{F}f(x, y, t)$. Then, (3.19) reads

$$\partial_t \hat{f}(k, y, t) + iky\hat{f}(k, y, t) = 0. \tag{3.20}$$

When we consider that k is a fixed parameter, the generator is $(-ik) \times \mathcal{X}$, where $\mathcal{X}$ denote the "coordinate operator"

$$\mathcal{X}\psi(x) = x\psi(x), \quad D(\mathcal{X}) = \{\psi;\ \psi(x), x\psi(x) \in L^2(\mathbf{R})\}. \tag{3.21}$$

On the contrary, when y is fixed, the generator is $(-iy) \times \mathcal{X}$. In both cases, the generator has continuous spectrum.

Let us define

$$E_q(\lambda)\psi(x) = \begin{cases} \psi(x) & \text{for } x \leq \lambda, \\ 0 & \text{for } x > \lambda. \end{cases} \tag{3.22}$$

For every $\varphi \in L^2(\mathbf{R})$, we have

$$\int_{-\infty}^{\infty} \lambda d(E_q(\lambda)\psi, \varphi) = \int_{-\infty}^{\infty} \lambda d\left(\int_{-\infty}^{\lambda} \psi(x)\overline{\varphi(x)}dx\right)$$

$$= \int_{-\infty}^{\infty} x\psi(x)\overline{\varphi(x)}dx = (\mathcal{X}\psi, \varphi).$$

Therefore, we may write

$$\mathcal{X} = \int_{-\infty}^{\infty} \lambda dE_q(\lambda). \tag{3.23}$$

We may formally write the generalized eigenfunction of $\mathcal{X}$ corresponding to a continuous spectrum λ as

$$\varphi_\lambda = \delta(x - \lambda),$$

where δ is Dirac's delta function.

We consider "correlations" of $\hat{f}(k, y, t)$ with some physical quantities $g(y)$ or $g(k)$;

$$\langle \hat{f}(k, y, t), g(y)\rangle_y \equiv \int_{-\infty}^{\infty} \hat{f}(k, y, t)\overline{g(y)}dy,$$

$$\langle \hat{f}(k, y, t), g(k)\rangle_k \equiv \int_{-\infty}^{\infty} \hat{f}(k, y, t)\overline{g(k)}dk.$$

Let us assume that k is fixed. Using the spectral resolution (3.22)-(3.23), the solution of (3.20), with initial value $\hat{f}_k(y) \in D(\mathcal{X})$, is given by

$$\hat{f}(k, y, t) = T(t)\hat{f}_k(y), \quad T(t) = \int_{-\infty}^{\infty} e^{-itk\lambda} dE_q(\lambda). \tag{3.24}$$

Therefore, we observe

$$\langle \hat{f}(k, y, t), g(y)\rangle_y = \int_{-\infty}^{\infty} e^{-itk\lambda} d\left[\int_{-\infty}^{\lambda} \hat{f}_k(y)\overline{g(y)}dy\right]$$

$$= \int_{-\infty}^{\infty} e^{-ityk} \hat{f}_k(y)\overline{g(y)}dy.$$

The most right-hand side is just the Fourier transform of $\hat{f}_k(y)\overline{g(y)}$ [$\in L^1(\mathbf{R})$]. By the Riemann-Lebesgue Theorem[1] we obtain $\lim_{t\to\infty}\langle \hat{f}(k, y, t), g(y)\rangle_y = 0$. Similar relation is obtained when we fix y. In summary we have

$$\lim_{t\to\infty} \langle \hat{f}(k, y, t), g(y)\rangle_y = 0, \quad (k \neq 0), \tag{3.25}$$

$$\lim_{t\to\infty} \langle \hat{f}(k, y, t), g(k)\rangle_k = 0, \quad (y \neq 0). \tag{3.26}$$

These relations are the mathematical representation of the phase-mixing damping (or the Landau damping).

[1] For $u(x) \in L^1(\mathbf{R})$, we have $\lim_{k\to\infty}(\mathcal{F}u)(k) = 0$.

3.4 Nonlinear effect and self-organization

The mixing effect in a linear system induces a continuous generation of complexity (inhomogeneity), and simultaneously, the relaxation into a homogeneous distribution in a coarse-grained sense. As a simple example, let us imagine a long-distance race on a track. If every runner goes with different speed, the dispersion of the group develops and finally, the distribution of runners on the track relaxes into a homogeneous distribution. However, in a real track event, we do not observe such a simple relaxation phenomenon. Each runner cares other people, and controls his speed. This introduces a nonlinear effect. Generally, we observe that runners make some groups. This is a typical "self-organization". A nonlinear effect cooperates with the mixing effect to produce structures in a complex system.

In the next section, we shall discuss the mixing of magnetic flux in a plasma, and the nonlinear effect of lorentz back-reaction that produces a structure of enhanced magnetic fields.

3.5 Example IV (MHD dynamo)

3.5.1 Constant-lambda Beltrami field

There are many different observations suggesting the creation of constant-λ Beltrami magnetic fields (force-free fields; Sec. 2.3) in astrophysical, space and laboratory plasmas. Magnetic flux tubes (flux ropes), in which field lines are twisted, are produced through interactions between the magnetosphere and interplanetary magnetic fields [11]. In a laboratory plasma, detailed measurements of magnetic fields showed that the field produced after self-organization through turbulence is closely approximated by a solution of (2.19) [14]. Galactic jets are also considered to have similar configurations of magnetic fields [7].

The constant-λ condition for the Beltrami field (Sec. 2.3) is a strong ansatz based on the following physical reasons. The streamline equation (2.21) in a three-dimensional magnetic field is generally non-integrable, and hence, we may assume that streamlines (magnetic field-lines) are embedded densely in a volume. Since (2.20) demands that λ is constant along each field line, it is natural to assume a constant λ over such a volume. The theory of energy relaxation also derives the constant-λ condition. Woltjer [18] pointed out the importance of the magnetic helicity

$$K = \frac{1}{2}\int_\Omega \boldsymbol{A}\cdot\boldsymbol{B}d\boldsymbol{x}.$$

Here $\nabla\times\boldsymbol{A}=\boldsymbol{B}$, Ω is the entire volume of the plasma and $d\boldsymbol{x}$ is the volume element. The viscous dissipation does not change the helicity K, while the magnetic energy diminishes toward a "ground state". The magnetic field self-organized through this energy relaxation is characterized by a minimizer of the magnetic energy $W = \int_\Omega B^2 dx/2$ subject to a given helicity. This variational principle reads as $\delta(W-\lambda K)=0$, where λ is the Lagrange multiplier. The formal Euler-Lagrange equation, under appropriate boundary conditions, is identical to (2.19). Taylor [14] formulated an equivalent variational principle, however, his model is based on a different hypothesis to justify the preferential conservation of the helicity. The energy dissipation proceeds faster than the change of the helicity, if the resistive dissipation is dominated by

spatially concentrated fluctuation currents (see also Hasegawa [5]). Both effects, the viscous dissipation, resulting in ion heating, and the resistive dissipation, resulting in electron heating, were compared for a specific relaxation process [21].

3.5.2 Fast dynamo

The Beltrami field plays an essential role in the so-called "dynamo theory". To understand the rapid generation of magnetic fields in astrophysical systems, we have to invoke a "fast dynamo action" that has a growth rate of the magnetic energy independent of the resistivity (see [17] and papers cited therein). In a highly conductive plasma the evolution of the magnetic field $\boldsymbol{B}$ obeys Faraday's law (2.18) with $\epsilon_L \to 0$. A plasma flow $\boldsymbol{v}$ with chaotic streamlines (maps with positive Lyapunov exponents), which may have a large length-scale, bring about complex mixing of magnetic flux, and the length-scale of the inhomogeneity cascades toward a small scale, resulting in amplification of the magnetic field. If the length-scale reduces down to the dissipative range, and the resistive damping becomes comparable to the induction effect, then the magnetic field energy turns to diminish. In this classical picture of the kinematic dynamo, the magnetic field energy accumulates into small scale fluctuations, and the life-time of the amplified magnetic field is limited by the time-scale of the cascade process. To obtain a larger length-scale and a longer life-time of amplified magnetic fields, an appropriate limitation for the scale reduction should occur. The nonlinear effect of the amplified magnetic fields, that is the Lorentz back-reaction, plays an essential role in this "post-kinematic phase". Here we assume that the plasma achieves a quasi-steady state through the energy relaxation process. Then, the momentum balance equation reduces into (2.19), and the flow $\boldsymbol{v}$ must be chosen in such a way that $\boldsymbol{B}$ satisfies (2.19) implicitly. The parameter λ characterizes the length-scales of $\boldsymbol{B}$. Hence, the condition (2.19) imposes a bound for the length-scale of the field, if the magnitude of λ is restricted by some reason. This bound avoids scale reduction down to the resistive regime, and extends the life-time of the amplified magnetic field.

Through the kinematic dynamo process, the current ($\propto \nabla \times \boldsymbol{B}$) tends to concentrate in small volumes, which may be disconnected. When the sectional length-scale of such a volume becomes small enough, the Lorentz force dominates ($\epsilon_A^2 \ll 1$). Let Ω to be such a "clump" of the magnetic field. Its length-scale is denoted by ℓ_c. This Ω may have a complex topology. We want to find a constant-λ Beltrami field in Ω. If the parameter λ can be chosen such that $|\lambda| \leq \lambda_c = O(\ell_c^{-1})$, then equilibration of the clump into such a Beltrami field results in a lower bound for the length-scale [26]. Here we solve the Beltrami condition (2.19) for a given helicity and an "external magnetic field". The external component of $\boldsymbol{B}$ is defined by decomposing $\boldsymbol{B} = \boldsymbol{B}_\Sigma + \boldsymbol{h}$, where $\nabla \times \boldsymbol{h} = 0$ and $\nabla \cdot \boldsymbol{h} = 0$. This $\boldsymbol{h}$, which represents the magnetic field rooted outside Ω, is assumed to be a given function. Its complement $\boldsymbol{B}_\Sigma$ is the unknown variable. We define the gauge-invariant helicity by

$$\mathcal{K} = \int_\Omega \boldsymbol{A} \cdot \boldsymbol{B}_\Sigma dx \tag{3.27}$$

We prove the existence of a solution with $|\lambda| \leq \lambda_c = O(\ell_c^{-1})$ for every $\boldsymbol{h} \neq 0$ and $\mathcal{K}$ in the next section (Theorem3). The nonvanishing $\boldsymbol{h}$ plays the role of symmetry breaking.

3.5.3 Spectral resolution of curl operator

The constant-λ Beltrami condition (2.19) is regarded as an eigenvalue problem with respect to the curl operator. Interestingly, the topology of the domain plays an essential role in this eigenvalue problem.

To study the spectrum the curl derivatives, we need the fundamental theory of vector function spaces. Let Ω ($\subset \boldsymbol{R}^3$) be a bounded domain with a smooth boundary $\partial\Omega = \cup_{i=1}^{n}\Gamma_i$ (Γ_i is a connected surface). We consider cuts of the domain Ω. Let $\Sigma_1, \cdots, \Sigma_m$ ($m \geq 0$) be cuts such that $\Sigma_i \cap \Sigma_j = \emptyset$ ($i \neq j$), and such that $\Omega \setminus (\cup_{i=1}^{m}\Sigma_i)$ becomes a simply connected domain. The number m of such cuts is the first Betti number of Ω. When $m > 0$, we define the flux through each cut by

$$\Phi_{\Sigma_i}(\boldsymbol{u}) = \int_{\Sigma_i} \boldsymbol{n} \cdot \boldsymbol{u} ds \qquad (i = 1, 2, \cdots, m),$$

where $\boldsymbol{n}$ is the unit normal vector on Σ_i with an appropriate orientation. By Gauss's formula, $\Phi_{\Sigma_i}(\boldsymbol{u})$ is independent of the place of the cut Σ_i, if $\nabla \cdot \boldsymbol{u} = 0$ in Ω and $\boldsymbol{n} \cdot \boldsymbol{u} = 0$ on $\partial\Omega$.

We denote $L^2(\Omega)$ the Lebesgue space of square-integrable (complex) vector fields in Ω, which is endowed with the standard innerproduct $(\boldsymbol{a}, \boldsymbol{b})$. We define the following subspaces of $L^2(\Omega)$;

$$L^2_\Sigma(\Omega) = \{\boldsymbol{w};\ \nabla \cdot \boldsymbol{w} = 0 \text{ in } \Omega,\ \boldsymbol{n} \cdot \boldsymbol{w} = 0 \text{ on } \partial\Omega,\ \Phi_{\Sigma_i}(\boldsymbol{w}) = 0\ (i = 1, \cdots, m)\},$$

$$L^2_H(\Omega) = \{\boldsymbol{h};\ \nabla \cdot \boldsymbol{h} = 0, \nabla \times \boldsymbol{h} = 0 \text{ in } \Omega,\ \boldsymbol{n} \cdot \boldsymbol{h} = 0 \text{ on } \partial\Omega\},$$

$$L^2_g(\Omega) = \{\nabla\phi\}.$$

We have an orthogonal decomposition [15]

$$L^2(\Omega) = L^2_\Sigma(\Omega) \oplus L^2_H(\Omega) \oplus L^2_g(\Omega).$$

The space of solenoidal vector fields with vanishing normal component on $\partial\Omega$ is

$$L^2_\sigma(\Omega) = L^2_\Sigma(\Omega) \oplus L^2_H(\Omega).$$

The subspace $L^2_H(\Omega)$ corresponds to the cohomology class, whose member is a harmonic vector field and $\dim L^2_H(\Omega) = m$ (the first Betti number of Ω). When Ω is simply connected, then $m = 0$ and $L^2_H(\Omega) = \emptyset$. We have the following theorems [20].

Theorem 1 *Let $\Omega \subset \boldsymbol{R}^3$ be a smoothly bounded domain. We define a curl operator $\mathcal{S}$ in the Hilbert space $L^2_\Sigma(\Omega)$ by*

$$\mathcal{S}\boldsymbol{u} = \nabla \times \boldsymbol{u}, \quad D(\mathcal{S}) = \{\boldsymbol{u} \in L^2_\Sigma(\Omega)\ ;\ \nabla \times \boldsymbol{u} \in L^2_\Sigma(\Omega)\}.$$

Then $\mathcal{S}$ is a self-adjoint operator. The spectrum of $\mathcal{S}$ consists of only point spectra $\sigma_p(\mathcal{S})$, which is a discrete set of real numbers.

Theorem 2 *In $L^2_\sigma(\Omega)$ we define a curl operator $\tilde{\mathcal{S}}$ by*

$$\tilde{\mathcal{S}} = \nabla \times \boldsymbol{u}, \quad D(\tilde{\mathcal{S}}) = \{\boldsymbol{u} \in L^2_\sigma(\Omega)\ ;\ \nabla \times \boldsymbol{u} \in L^2_\sigma(\Omega)\}.$$

(i) When $\dim L^2_H(\Omega) = 0$, *i.e. if* Ω *is simply connected, then* $\tilde{S} \equiv S$, *and hence, the spectrum* $\sigma(\tilde{S}) = \sigma_p(\tilde{S})$.

(ii) When $\dim L^2_H(\Omega) > 0$, *i.e. if* Ω *is multiply connected, then* $\tilde{S}$ *is an extension of* S. *The spectrum* $\sigma(\tilde{S})$ *consists of only spectra* $\sigma_p(\tilde{S})$, *and* $\sigma_p(\tilde{S}) = \mathbf{C}$. *Hence, for every* $\lambda \in \mathbf{C}$,

$$(\tilde{S} - \lambda)\boldsymbol{u} = 0 \tag{3.28}$$

has a nontrivial solution.

Theorem 2 proves the general existence of the constant-λ Beltrami function for every $\lambda \in \mathbf{C}$, if Ω is multiply connected. In the next theorem, we solve the constant-λ Beltrami equation (2.19) for a given helicity $\mathcal{K}$ and harmonic field $\boldsymbol{h} \in L^2_H(\Omega)$. Now λ is an unknown variable. This problem is related with the magnetic clump discussed in Sec. 2.

3.5.4 Topological genus and topological symmetry breaking

We assume that Ω is multiply connected. Let $\{\varphi_j\}$ be the complete set of the eigenfunctions of the self-adjoint curl operator S (Theorem 1). The corresponding eigenvalues are numbered as

$$\cdots \leq \mu_{-2} \leq \mu_{-1} < 0 < \mu_1 \leq \mu_2 \leq \cdots. \tag{3.29}$$

For every $\boldsymbol{B} \in L^2_\sigma(\Omega)$, we have an orthogonal-sum expansion

$$\boldsymbol{B}(\boldsymbol{x}, t) = \sum_j c_j(t)\varphi_j(\boldsymbol{x}) + \boldsymbol{h}(\boldsymbol{x}, t), \tag{3.30}$$

where $\boldsymbol{h} \in L^2_H(\Omega)$. The harmonic field $\boldsymbol{h}$ is a given function, which plays an important role of "symmetry breaking" in the following discussion. The first summation in the right-hand side of (3.30) is denoted by $\boldsymbol{B}_\Sigma$. The energy of $\boldsymbol{B}$ is given by

$$W = \frac{1}{2}\sum_j c_j^2 + \frac{1}{2}\|\boldsymbol{h}\|^2. \tag{3.31}$$

There exists $\boldsymbol{g}$ such that $\boldsymbol{h} = \nabla \times \boldsymbol{g}$. The vector potential of $\boldsymbol{B}$ is given by

$$\boldsymbol{A} = \sum_j \frac{c_j}{\mu_j}\varphi_j + \boldsymbol{g}. \tag{3.32}$$

Denoting $D_j = (\varphi_j, \boldsymbol{g})$, the gauge invariant helicity (3.27) becomes

$$\mathcal{K} = \frac{1}{2}(\boldsymbol{A}, \boldsymbol{B}_\Sigma) = \frac{1}{2}\sum_j (\frac{c_j^2}{\mu_j} + D_j c_j). \tag{3.33}$$

For given $\mathcal{K}$ and $\boldsymbol{h}$, we can solve (2.19) by the variational principle $\delta(W - \lambda\mathcal{K}) = 0$, and obtain

$$c_j = \frac{\lambda\mu_j}{2(\mu_j - \lambda)} D_j \quad (\forall j). \tag{3.34}$$

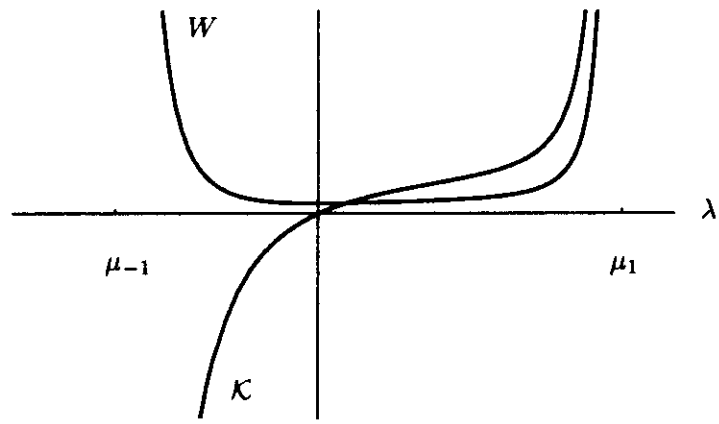

Figure 3.3: Typical graphs of the energy $W(\lambda)$ and the helicity $\mathcal{K}(\lambda)$ (arbitrary units). For every $\mathcal{K}_0$, the equation $\mathcal{K}(\lambda) = \mathcal{K}_0$ has a unique solution in the range of $\mu_{-1} < \lambda < \mu_1$.

The energy and the helicity become

$$W = \sum_j \frac{\lambda^2 \mu_j^2}{8(\mu_j - \lambda)^2} D_j^2 + \frac{1}{2}\|\boldsymbol{h}\|^2, \qquad \mathcal{K} = \sum_j \frac{\lambda \mu_j (2\mu_j - \lambda)}{8(\mu_j - \lambda)^2} D_j^2. \tag{3.35}$$

We can show that $\mathcal{K}$ is a monotone function of λ in the range of $\mu_{-1} < \lambda < \mu_1$ (see definition (3.29) and Fig. 3.3), if $D_j \neq 0$ $(\exists j)$, viz., if we have a "symmetry breaking" $\boldsymbol{h} \neq 0$. For every $\kappa \in \mathbf{R}$, the equation $\mathcal{K}(\lambda) = \kappa$ has a unique solution in this range of λ. Now we have the following theorem.

Theorem 3 *Let Ω $(\subset \mathbf{R}^3)$ be a multiply connected bounded domain. Assume that $\boldsymbol{h}$ $(\in L^2_H(\Omega))$ is finite. For every κ $(\in \mathbf{R})$, the Beltrami condition (2.19) has a unique solution $\boldsymbol{B}$ such that its helicity $\mathcal{K} = \kappa$, and λ such that $\mu_{-1} < \lambda < \mu_1$.*

3.5.5 Invariant measure and statistical ensemble

Using the phenomenological variational principle $\delta(W - \lambda\mathcal{K}) = 0$ (Sec. 2), we develop a statistical mechanical model that reproduces the constant-λ Beltrami field at the "zero *temperature* limit". A finite *temperature* (in the sense of MHD fluctuation) equilibrium includes fluctuations. The statistical theory predicts the spectra of macroscopic physical quantities such as the energy, helicity, etc.

A key step is to find an invariant measure of the temporal evolution equation. It corresponds to Liouville's theorem in the Hamiltonian dynamics. Montgomery *et al.* [10] used the

"Chandrasekhar-Kendall functions", which are the eigenfunctions of the curl in a cylindrical geometry [2], to expand the solenoidal vector fields $\boldsymbol{B}$ and $\boldsymbol{v}$, and defined an infinite-dimensional phase space spanned by the expansion coefficients. The formal Lebesgue measure is shown to be invariant against the nonlinear ideal ($\epsilon_R, \epsilon_L \to \infty$) dynamics. The completeness theorem of the eigenfunctions (Theorem 1) gave a mathematical justification of the expansion, and generalized the Hilbert-space approach for an arbitrary geometry. An important development in recent work [6] is the treatment of the harmonic magnetic field, which brings about a symmetry breaking associated with a topological constraint. When we consider a multiply connected domain, the harmonic magnetic fields, which are rooted outside the domain, are represented by the cohomology class. If we impose the ideal conducting boundary conditions, these harmonic fields are invariant. The rest orthogonal complement spans the dynamical phase space. The invariant harmonic component plays the role of an externally applied symmetry breaking. Interestingly, this term yields "power-law spectra" of the energy, helicity and helicity fluctuation. It is easy to verify the following proposition.

Proposition 1 (Invariant Measure) *Let $\boldsymbol{v}(x,t)$ be a smooth vector field in Ω. Suppose that $\boldsymbol{B}(x,t)$ obeys*

$$\partial_t \boldsymbol{B} = \nabla \times (\boldsymbol{v} \times \boldsymbol{B}) \quad \text{in } \Omega, \tag{3.36}$$

$$\boldsymbol{n} \times (\boldsymbol{v} \times \boldsymbol{B}) = 0 \quad \text{on } \partial\Omega. \tag{3.37}$$

Using the eigenfunctions of the curl operator φ_j and the harmonic field $\boldsymbol{h}_\ell$, we write $\boldsymbol{B}(x,t)$ in the form of (3.30). Then, $dC = \prod_j dc_j$ is an invariant measure.

(proof) By the boundary condition (3.37), we observe $d\check{c}_\ell/dt = 0$ $(\forall \ell)$. Using (3.36) and (3.37), we obtain

$$\frac{d}{dt}c_j = (\nabla \times (\boldsymbol{v} \times \boldsymbol{B}), \boldsymbol{\varphi}_j) = (\boldsymbol{v} \times \boldsymbol{B}, \nabla \times \boldsymbol{\varphi}_j) = \lambda_j (\boldsymbol{v} \times \boldsymbol{B}, \boldsymbol{\varphi}_j)$$

$$= \lambda_j \left[\sum_k c_k (\boldsymbol{v} \times \boldsymbol{\varphi}_k, \boldsymbol{\varphi}_j) + \sum_{\ell=1}^{m} \check{c}_\ell (\boldsymbol{v} \times \boldsymbol{h}_\ell, \boldsymbol{\varphi}_j) \right]. \tag{3.38}$$

Since $(\boldsymbol{v} \times \boldsymbol{\varphi}_j) \cdot \boldsymbol{\varphi}_j \equiv 0$, we find $\partial(dc_j/dt)/\partial c_j = 0$ $(\forall j)$. Hence the measure dC is invariant.

(Q.E.D.)

The ansatz of the variational principle $\delta(W - \lambda \mathcal{K}) = 0$ suggests that two additive quantities W and $\mathcal{K}$ are the relevant state variables that characterize the statistical equilibrium. The possible ensemble consistent with this variational principle is the Boltzmann distribution

$$P(W, \mathcal{K}) \propto \exp[-\beta(W - \lambda \mathcal{K})] \tag{3.39}$$

where β is interpreted as an inverse temperature of the magnetic field. The helicity and the energy of each mode is $(c_j^2/\mu_j + D_j c_j)/2$ and $c_j^2/2$, respectively. The Boltzmann distribution

for the amplitude c_j is

$$P_j \propto \exp\left[-\frac{\beta}{2}\left(c_j^2 - \frac{\lambda}{\mu_j}c_j^2 - \lambda D_j c_j\right)\right]. \tag{3.40}$$

The ensemble averages of W and $\mathcal{K}$ over the phase space become

$$\langle W\rangle = \sum_j \left[\frac{\mu_j}{2\beta(\mu_j-\lambda)} + \frac{\lambda^2\mu_j^2}{8(\mu_j-\lambda)^2}D_j^2\right], \tag{3.41}$$

$$\langle \mathcal{K}\rangle = \sum_j \left[\frac{1}{2\beta(\mu_j-\lambda)} + \frac{\lambda\mu_j(2\mu_j-\lambda)}{8(\mu_j-\lambda)^2}D_j^2\right]. \tag{3.42}$$

These results are compared with (3.35). The first term of the right-hand side of (3.41) and that of (3.42) are the contributions of the fluctuations. In (3.41), the energy of the harmonic field, which is constant here, is omitted. This classical statistical model suffers from the Rayleigh-Jeans catastrophe, viz., when we pass the limit of the infinite summation over the all modes, the fluctuation terms diverge. To avoid this divergence, we can appeal to the Bose-Einstein statistics with second-quantizing the mode amplitude c_j and defining bosons MHD fluctuations [6].

Bibliography

[1] BOOZER A. H., *J. Plasma Phys.* **35**, 133-139 (1986).

[2] CHANDRASEKHAR S. & KENDALL P. C., *Astrophys. J.* **126**, 457-460 (1957).

[3] GRAD, H. & RUBIN, H., in *Second United Nation Conference on the Peaceful Uses of Atomic Energy*, Vol. 31, pp. 190-197. IAEA, Geneva (1958).

[4] GRAD H. & VAN NORTON R., *Nucl. Fusion* (1962) 1962 Suppl. Part 1, p. 61.

[5] HASEGAWA A., *Adv. Phys.* **34**, 1-42 (1985).

[6] ITO N. & YOSHIDA Z., *Phys. Rev. E* **53**, 5200-5206 (1996).

[7] KŌNIGL A. & CHOUDHURI A. R., *Astrophys. J.* **289**, 173-187 (1985).

[8] KOWALSKI K. & STEEB W. H., *Nonlinear Dynamical Systems and Carleman Linearization*, World Scientific, Singapore (1991).

[9] LADYZHENSKAYA O. A. & SOLONNIKOV V. A., *J. Soviet Math.* **8**, 384-422 (1977).

[10] MONTGOMERY D., TURNER L. & VAHALA G., *Phys. Fluids* **21**, 757-764 (1978).

[11] RUSSEL C. T., in *Magnetic Reconnection in Space and Laboratory Plasmas*, (Ed. E. W. Hones), pp. 124-138. American Geophysics Union, Washington DC (1984).

[12] SCHMIDT G., *Phys. Fluids* **5**, 994 (1962).

[13] STRAUSS H. A., *Phys. Fluids* **29**, 3668-3671 (1986).

[14] TAYLOR J. B., *Phys. Rev. Lett.* **33**, 1139-1141 (1974).

[15] TEMAM R., *Navier-Stokes Equations*, North-Holland, Amsterdam (1984).

[16] UCHIDA T, *Jpn. J. Appl. Phys.* **33**, L43 (1994).

[17] VAINSHTEIN S. I., SAGDEEV R. Z., ROSNER R. & KIM E.-K., *Phys. Rev. E* **53**, 4729-4744 (1996).

[18] WOLTJER L., *Proc. Natl. Acad. Sci. U.S.A.* **44**, 489-491 (1958).

[19] YOSHIDA Z. & GIGA Y., *J. Math. Phys.* **24**, 2860-2864 (1983).

[20] YOSHIDA Z. & GIGA Y., *Math. Z.* **204**, 235-245 (1990).

[21] YOSHIDA Z., *Nucl. Fusion* **31**, 386-390 (1991); YOSHIDA Z. & HASEGAWA A., *Phys. Fluids B* **4**, 3013-3015 (1992).

[22] YOSHIDA Z., SAKURAGI Y. & YAMAKOSHI Y, *J. Plasma Phys.* **49**, 403-411 (1993).

[23] YOSHIDA Z., *Phys. Plasmas* **1**, 208-209 (1994).

[24] YOSHIDA Z., in *Current Topics in the Physics of Fluids*, Vol. 1, pp. 155-178. Council of Scientific Information, Trivandrum (1994).

[25] YOSHIDA Z. & UCHIDA T., *Jpn. J. Appl. Phys.* **34**, 4213- (1995); ASAKURA H., TAKEMURA, K., YOSHIDA Z. & UCHIDA T., *Jpn. J. Appl. Phys.* **36**, 4493-4496 (1997).

[26] YOSHIDA Z., *Phys. Rev. Lett.* **77**, 2722-2725 (1996).